Multiple Pulses in dE/dt and the Fine-Structure of E During the Onset of First Return Strokes in Cloud-to-Ocean Lightning

Natalie D. Murray, E. Philip Krider, and John C. Willett

Institute of Atmospheric Physics
The University of Arizona
Tucson, Arizona 85721-0081
U.S.A.

Revised 11 August 2004

Abstract

We have analyzed the fine-structure of 131 electric field (E) waveforms that were radiated during the onset of first return strokes in cloud-to-ocean lightning. The dE/dt waveforms were recorded using an 8-bit waveform digitizer sampling at 100 MHz, and the E waveforms were sampled at 10 MHz using a 10-bit digitizer. 49 (or 37%) of the dE/dt waveforms contain one or more large pulses within ±1 μs of the largest (or dominant) peak in dE/dt, i.e. within an interval from -1 μs to +1μs, where t = 0 μs is the time of the dominant peak, and 37 (or 28%) have one or more large pulses in the interval from 4 μs before to 1 μs before the dominant peak, i.e. -4 μs to –1 μs, and only the dominant peak within ± 1 μs . We give statistics on the amplitude and timing of dE/dt pulses that are near the dominant peak, and we show how the presence of these pulses adds considerable fine-structure to the shape of E_{int}, the integrated dE/dt waveform, on a time-scale of tens to hundreds of nanoseconds. This fine-structure includes fast pulses near the beginning of the slow front, large pulses and shoulders within the slow front and during the fast transition, and very narrow peaks in E_{int}. Our overall conclusion is that the electromagnetic environment near the point(s) where lightning leaders attach to the surface is often more complicated than what would be produced by a single current pulse propagating up a single channel at the time of onset.

1.0 INTRODUCTION

Submicrosecond measurements of the electric field, E, and dE/dt waveforms that are radiated during the onset of first return strokes in cloud-to-ocean lightning have been reported previously by Weidman and Krider (1978; 1980; 1984), Krider et al. (1996), Willett et al. (1995; 1998), and Willett and Krider (2000). Weidman and Krider (1978; 1980) noted that the shape of the initial E field, when recorded under conditions where there is minimal distortion due to the effects of ground-wave propagation, typically begins with a slow, concave front that lasts for several microseconds. The front is followed by a fast-transition to the peak E, and then there are a variety of subsidiary peaks and other features that are thought to be due to the effects of branches, the complex geometry of the channel, and/or traveling waves of current during the attachment process (Weidman and Krider, 1978; Weidman et al., 1986; Willett et al., 1988; Leteinturier et al., 1990). In the discussion of their Fig. 2c to 2f, Weidman and Krider (1978) noted that sometimes the slow front has a convex shape, rather than concave, and they hypothesized that this might be due to the impulse from a leader step being superimposed on the initial rise of the return stroke field. Willett and Krider (2000) reported that 39% of their first stroke waveforms had multiple pulses in dE/dt near the time of the fast-transition in E (see their Fig. 3), and they noted that E waveforms obtained by numerically integrating their dE/dt records (100 MHz sampling) sometimes contained very narrow, fast peaks not resolved by an E waveform digitizer sampling at 10 MHz. Given the above and

the relative paucity of waveform measurements on natural lightning with very fast time-resolution, we have re-examined the fine-structure of the dE/dt and E waveforms in the dataset described by Willett et al. (1998) and Willett and Krider (2000) with the goal of quantifying this structure on a time-scale of tens to hundreds of nanoseconds.

2.0 DATA

Our database comprises 131 dE/dt and E waveforms that were recorded in 1985 just north of the NASA Kennedy Space Center (KSC) on Playalinda Beach, Florida (Willett et al., 1998). The lightning locations were measured using a network of three gated, wideband magnetic direction-finders (Krider et al., 1980) that provided an overall location accuracy of about 1 km (Maier and Jafferis 1985; Krider et al. 1996). The flashes occured at ranges of 5 to 50 km on three thunderstorm days, and maps showing the locations of the experiment site and the lightning strike points are given in Willett et al. (1990, Fig. 2) and Willett et al. (1998, Figs. A2, A3, and A4). Three independent flush plate antennas mounted on the roof of a well-grounded metal trailer were used to measure the E, dE/dt, and RF signals produced by the lightning. The trailer housed the recording electronics and was parked about 45 m from the Atlantic Ocean so that any fields originating from lightning over the ocean would be measured with minimal distortions due to the effects of propagation over the ocean/land surface (Cooray and Ming, 1994; Cooray, 2003, Chapter 7; Cooray et al., 2004).

Indeed, Krider et al. (1996) have previously argued that E and dE/dt measurements made at a similar site in 1984 were not significantly affected by

propagation. Willett et al. (1998, Table 1) also showed that the mean peak dE/dt in 1985 was comparable to that in 1984, and that the full-width-at-half-maximum (FWHM) of the initial half-cycle of dE/dt in 1985 had a mean that was comparable to, or possibly even slightly *less,* than that in 1984. Because the waveform measurements in 1985 were at comparable ranges to those in 1984 and produced similar results, we believe that there are minimal distortions in the 1985 waveforms due to the effects of propagation. This issue will be examined further in section 5.5.

A block schematic diagram of the data acquisition system has been given by Willett et al. (1989, Fig. 1). dE/dt waveforms were digitized using an 8-bit A/D converter sampling at 100 MHz, and E waveforms were digitized using a 10-bit A/D converter sampling at 10 MHz. The effective bandwidths of the dE/dt and E recording systems were about 30 MHz and 3 MHz, respectively. Both digitizers were triggered on the output of a wideband RF receiver tuned to 5 MHz in order to minimize any biases that might be introduced by the finite trigger threshold. Krider et al. (1996) and Willett et al. (1998) have given detailed discussions of the possible trigger biases in 1984 and 1985, respectively. No evidence has been found for a range-dependence in the values of the range-normalized peak dE/dt, and there is no indication that the values of FWHM have been biased by the RF triggering technique.

Plots of all dE/dt and E waveforms in our dataset, together with the outputs of the RF receiver and the slow-E antenna, are given in technical reports by Bailey and

Willett (1989) and Izumi and Willett (1991). The type of lightning process that triggered the recording system was determined from the overall shape and structure of the E and slow-E waveforms. All CG flashes in our dataset effectively lowered negative charge toward ground, and the initial E fields were negative or downward transitions following the physics sign convention. The amplitudes of all waveforms given in this paper have been range-normalized to 100 km, assuming that the radiated field has an inverse-distance dependence on range and that any attenuation of high frequencies by propagation over the ocean surface and the narrow strip of land is negligible.

3.0 CHARACTERISTICS OF dE/dt AND E WAVEFORMS

The primary focus of this paper will be on a 5 μs interval that corresponds to the onset of first stroke waveforms, i.e. the slow front, the fast-transition, and the initial peak of E. We start by examining the number and timing of large pulses that appear in the dE/dt records, and we then consider the effects that these pulses have on the fine-structure of E. Any deviations from the normal or "classical" shapes (e.g., Weidman and Krider, 1978) will be noted and further classifications will be assigned as necessary.

To determine the fine-structure of E, each dE/dt record (100 MHz) has been numerically integrated over a 15 μs interval that includes the peak E to provide a waveform that we designate E_{int}. This integration has been done using the trapezoidal rule, and because the shape of E_{int} is very sensitive to small offsets in

dE/dt, we systematically stepped through a number of offsets and then selected the one that provided the best least-squares fit to the measured 10 MHz E waveform. (The results of this procedure are shown in red in Fig. 1b, 2b, and 4 through 13 to follow and will be discussed in detail below.) In order to keep the effects of any residual baseline offsets from affecting the values of peak E_{int} (given in Table 1 and Fig. 14 to follow), we also averaged E_{int} over the first 5 μs of the 15 μs integrating interval (typically including only a few leader steps) and then subtracted this average from the value of the peak E_{int}. Additionally, because the time differentiation inherent in a dE/dt recording causes any information about the variations in E below some frequency to fall below the lowest level of digitizer resolution, E_{int} occasionally exhibits spurious low-frequency features that do not match the (correct) behavior that is preserved in the 10 MHz E record (e.g., Fig. 4). Because of this, we also visually compared the offset of E_{int} at – 4 μs (the origin of our time-scale will be discussed in section 3.2) with the corresponding 10 MHz E record and subtracted the difference from the value of the peak E_{int}. (One example of this zero level correction is illustrated by the horizontal green line in Fig. 4 to follow.)

3.1 Single Peak dE/dt Waveforms (Type A)

Fig. 1a shows the initial portion of a “classical” E waveform from a first return stroke together with the corresponding dE/dt signature. Events like this, which produce a single large pulse in dE/dt corresponding to the fast-transition in E, will be termed “Type A” strokes. The same waveform as in Fig. 1a is shown on an expanded time scale in Fig. 1b. Here E_{int} signature has been plotted in red

together with the individual samples of E (asterisks). Our term “pulse in dE/dt” usually refers to an isolated negative impulse that is immediately followed by a positive overshoot, as shown in the upper panel of Fig. 1b. We define the “dominant peak” in dE/dt to be the largest negative-going pulse that occurs during the fast-transition in E. Note that, in Fig. 1b, how the origin of the time-axis has been shifted to coincide with the time of the dominant peak.

3.2 Multiple Peak dE/dt Waveforms

Fig. 2 shows records similar to Fig. 1, but for a stroke that produced multiple pulses in dE/dt near the time of the peak E. Since multiple pulses were present in a significant fraction of our dE/dt records, we will now examine the characteristics of these features in more detail.

In order to classify the dE/dt waveforms, we counted pulses if they had: (a) a (negative) peak amplitude that was at least 10% of the amplitude of the largest or dominant peak and (b) the (positive-going) return of that signal toward the baseline reached a (negative) level that was 50% of its own (negative) peak amplitude. Strokes that had multiple pulses in dE/dt were further classified according to the time of any additional pulse (or pulses) relative to the dominant peak. Here we will focus primarily on pulses that occur in the 5 μs interval from -4 μs to +1 μs, i.e., 4 μs before to 1 μs after the dominant peak, and we will assume that all pulses prior to –4 μs, a typical duration of the slow front (Weidman and Krider, 1978; 1980), were produced by the final steps of the stepped-leader process that initiated the stroke rather than by the onset of the

stroke itself (Krider et al., 1977). Of course, some of the pulses which occurred after -4 μs could be due to leader steps, and we will consider this point further in section 3.3.

Fig. 3 summarizes the characteristics of all dE/dt pulses that satisfied the above selection criteria and that occurred in a 10 μs interval containing the dominant peak (i.e. –9 μs to +1 μs). Fig. 3a gives the number of pulses (excluding the dominant peak) in consecutive one microsecond time bins, and Fig. 3b shows the mean (negative) amplitude of these pulses relative to that of the dominant peak. Fig. 3c shows an example of the types of pulses that were included in Fig. 3a and 3b.

Within our total sample of 131 first return strokes, each having a dominant peak, 49 (or 37%) produced one or more pulses in dE/dt (in addition to the dominant peak) within ± 1 μs of the dominant peak, and these events will be termed “Type B” strokes. 37 (or 28%) of first strokes produced one or more pulses in the interval from –4 μs to – 1 μs before the dominant peak (and no pulse within ± 1 μs of the dominant peak). These events will be termed “Type C” strokes. Thus, there are a total of 86 first strokes – an astonishing 66% of the total – that produced multiple pulses in dE/dt in a 5 μs interval near the dominant peak in dE/dt (and the peak E). (Although not directly noted above, all first stroke waveforms in our dataset had considerable fine-structure after the initial peak E, i.e., α-peaks and other subsidiary features termed a, b, c by Weidman and Krider (1978; 1980).)

3.2.1 Type B Events

The 49 Type B events produced a total of 136 large pulses in dE/dt (in addition to the dominant peak) within ± 1 μs of the dominant peak; therefore, the average number of pulses between -1 μs and 1 μs in Type B strokes was (136+49)/49 or 3.8, including the dominant peak. It should be noted that the average amplitude of the extra pulses in Type B strokes was about 40% of the dominant peak (see Fig. 3b). Fig. 2 and 4 to 7 to follow show examples of the dE/dt and E_{int} waveforms produced by Type B strokes.

3.2.2 Type C Events

The 37 events classified as Type C strokes produced a total of 85 pulses in dE/dt in the interval between –4 μs to –1 μs relative to the dominant peak and no additional pulses in the interval from ±1 μs except the dominant peak. Thus the average number of dE/dt pulses in Type C strokes was (85+37)/37 or 3.3, including the dominant peak. (Note: some of the Type B strokes also had pulses between –4 μs and –1 μs, and although such pulses are not counted here, they are counted in Fig. 3.) Fig. 8 to 12 give examples of the dE/dt and E_{int} waveforms produced by Type C strokes.

3.3 Leader Step Waveforms

Practically all events in our dataset showed evidence of E and dE/dt radiation from the final steps of the stepped-leader process that preceded the onset of the first return stroke. The shapes of the leader dE/dt pulses tend to fall into two broad categories: (a) a single large impulse, which we term a "leader step" or LS waveform and (b) a short burst of smaller pulses which we term a "leader burst" or LB signature. The integral of both types of dE/dt waveforms produces an almost unipolar E signature with a duration of about one microsecond. (See Krider et al.,1977, and Willett and Krider, 2000, for further discussions of leader step waveforms.) In our total sample of 131 first stroke waveforms, 48 (or 37%) had an LS impulse in the 5 μs interval from -9 μs to -4 μs before the dominant peak, and 75 (or 57%) had a LB in that interval. Many examples of LS and LB waveforms can be seen in Fig. 2 to 13, and specific examples have been labeled in Fig. 2b, 8, 9, 11 and 13. As we will see, many of the waveforms that contain multiple pulses in dE/dt between -4 μs and 1μs could be the result of large LS and/or LB waveform(s) being superimposed on the onset of the return stroke field. Further details about the characteristics of LS and LB waveforms will be given in a future paper.

4.0 FINE-STRUCTURE OF THE E_{INT} WAVEFORMS

We have seen that the dE/dt signatures radiated during the onset of first return strokes can be broadly classified into: Type A events that have a single, negative (dominant) peak in a 5 μs interval that contains the peak E; Type B events that have one or more additional pulses within ±1 μs of the dominant peak; or Type C

events that have a dominant peak and at least one additional pulse in the interval from –4 μs to –1 μs, and no additional pulses within ± 1 μs of the dominant peak. The shapes of the corresponding E_{int} waveforms have reproducible features that depend upon the amplitude and timing of the dE/dt pulses relative to the dominant peak.

4.1 Type A Events

Strokes with a single, dominant peak in dE/dt tend to produce the "classical" E_{int} waveform as described by Weidman and Krider (1978), i.e., a slow, concave front followed by a fast-transition to peak, and little additional structure. The E_{int} waveforms in Fig. 1 and Fig. 13 are typical Type A signatures.

4.2 Type B Events

The E_{int} waveforms for Type B strokes tend to have an inflection point (or shoulder) within or near the fast (negative-going) transition in E_{int} or, if the additional dE/dt pulse contains a (positive-going) zero crossing, there are multiple peaks in E_{int}. We term any such peaks or shoulders "γ-peaks" or "γ-shoulders," and, of course, such features can occur either near the beginning, in the middle (Fig. 4), or toward the end (Fig. 5) of the fast-transition, depending on the relative amplitude and timing of the pulses in dE/dt. Fig. 6 shows two well-defined γ-peaks that are very narrow (less than 0.2 μs). Here, the effect of multiple pulses in dE/dt is to produce a 0.5 μs delay between the dominant peak (in dE/dt) and the peak E_{int}. Of the 49 Type B strokes in our dataset, 31 produced a total of 34 γ-peaks, and all except one had one or more γ-shoulders. The waveform shown in Fig. 9 (discussed further below) has a feature similar to

a γ-peak just after the peak E_{int}. Weidman and Krider (1978) noted features similar to γ-shoulders, but to the best of our knowledge, γ-peaks have not been previously reported in the lightning literature.

Fig. 7 shows an unusual dE/dt waveform and the associated E_{int} and E signatures. Note here how there are five large pulses in dE/dt (not including the dominant peak), three negative and two positive, in the 2 μs interval before the dominant peak. The time between the dominant peak in dE/dt and the next largest negative peak is 0.84 μs, which places this waveform in our Type B category. The corresponding E_{int} signature contains a very fast and narrow negative impulse followed by a distinct shoulder lasting about 0.8 μs, and then there is a second fast-transition to the peak E_{int}. The dominant peak in dE/dt is quite narrow, and the corresponding peak in E_{int} is also narrow and small. Note that the largest negative peak in dE/dt prior to the dominant peak has a peak amplitude that is 87% that of the dominant peak.

4.3 Type C Events

Type C strokes are those that contain one or more large pulses in dE/dt near the beginning or during the slow front, and the corresponding E_{int} signatures have a structure that depends on the amplitude and duration of these pulses (or bursts) and when they occur relative to the dominant peak. Fig. 8 shows a dE/dt waveform (Type C) with a large pulse at about –3.7 μs, near the beginning of the slow front, and the corresponding E_{int} waveform contains a fast, unipolar pulse at this time. The complex cluster of dE/dt pulses between –4.5 μs and – 5.5 μs is

what we are terming a “leader burst,” and note how the corresponding E_{int} waveform is almost unipolar. There were 15 waveforms of the type shown in Fig. 8 in our dataset.

Four strokes produced large pulses in dE/dt during the development of the slow front, and these tended to produce E_{int} waveforms like that shown in Fig. 9. Two strokes produced bursts of dE/dt pulses during the slow front, and the corresponding front in E_{int} was convex as shown in Fig. 10. Seven strokes produced multiple pulses in dE/dt during the front, and Fig. 11 shows how such pulses create an abrupt negative transition or a shoulder in E_{int} that is followed by a slower, clearly defined plateau prior to the fast-transition. Fig. 12 shows how a burst of 3 dE/dt pulses at - 2 μs created an abrupt shoulder in E_{int}.

5.0 DISCUSSION

5.1 Narrow Peaks in E_{int}

Fig. 13 shows an example of an E_{int} waveform that has a very narrow peak which was not resolved by the 10 MHz E digitizer (see also Fig. 2b, 4, 7 and 8). Since narrow peaks were a fairly common feature in our data set, and since the values of peak E are often used to infer the peak current in first return strokes (Rakov and Uman, 1998; Cummins et al., 1998a,b), we have compared the values of peak E_{int}, obtained by integrating dE/dt waveforms (100 MHz sampling), with the values of peak E obtained from the 10 MHz E digitizing system. Table 1 and Fig. 14 summarize the results for all Type A, B, and C strokes in our dataset. Note in

Fig. 14 that 13 strokes (10% of the total) have a peak E_{int}/peak E ratio equal to or greater than 1.15, the maximum is 1.31, and the mean is 1.07. The values of the peak E_{int} and peak E (range-normalized to 100 km) in Table 1 have an overall mean and standard deviation (SD) of -9.0 $\pm$ 4.4 V/m and -8.6 $\pm$ 4.4 V/m, respectively, and the median peak E_{int} and peak E are –7.9 V/m and -7.2 V/m, respectively. It should also be noted in Table 1 that the integrated effect of multiple peaks in dE/dt (Type B strokes) is to produce a mean amplitude that is about 40% larger than that of the single-peak (Type A) strokes.

To quantify the width of the fast peaks in E_{int}, we have measured the time-interval between the dominant (negative) peak in dE/dt and the peak of the (positive) overshoot that immediately follows the dominant peak in 114 events where the dominant peak corresponded to the fast-transition in E_{int} and where the positive overshoot in dE/dt had a well-defined peak (see, for example, Fig. 13) and events like those shown in Fig. 5 and 6 were omitted. The results are shown in Fig. 15. Note that the intervals in Fig. 15 range from 0.04 μs to 0.26 μs (with a digitizer resolution of 0.01 μs). The mean and SD are 0.11 $\pm$ 0.04 μs, and the median is 0.10 μs. 70 (or 60%) of the 114 strokes in Fig. 15 had an interval (as defined above) that was less than 0.12 μs; therefore, any digitizing system that samples E at a frequency of 10 MHz or less (i.e., a sampling interval of 0.1 μs or greater) will not be capable of resolving the true peak field or the other fine-structure that is often present in E during the onset of first strokes.

Fig. 16 shows the amplitude of the positive overshoot in dE/dt relative to the dominant (negative) peak for the 114 strokes that have been plotted in Fig. 15. The mean and SD of these ratios are 0.27 ± 0.16, the median is 0.26, and 86% of the overshoot amplitudes are less than 40% of the dominant peak.

One possible explanation for the very narrow peaks in E_{int} has been suggested by Leteinturier et al. (1990); namely, if the first return stroke begins at an elevated junction point between the upward connecting discharge and the last step of the downward-propagating stepped-leader, traveling waves of current might propagate both upward and downward from this point until the downward wave is partially reflected at the surface. During the time when there are both upward and downward propagating waves, the radiated field could be up to a factor of two larger than what would be radiated after the partial reflection (see, for example, Fig. 17 in Leteinturier et al. (1990) and the discussion in Cooray et al. (2004)).

5.2 Peak E vs. Peak dE/dt

Fig. 17 shows plots of the peak E_{int} vs. the (dominant) peak dE/dt for all Type A, B, and C strokes in our dataset. Note that the values for the Type A and Type C strokes are moderately well correlated (R^2 values of 0.501 and 0.503, respectively) but with different slopes. Type B strokes have little correlation (R^2 = 0.013), presumably because the peak E_{int} is dominated by the integrated effects of the multiple pulses in dE/dt. The slope of the Type A fit is similar to, but not directly comparable with, that of Willett and Krider (2000, Fig.5), who excluded all

Type B waveforms and some Type C waveforms from their analyses and then compared the peak dE/dt to the amplitude of the fast-transition in E (i.e., the slow front was omitted). The slopes of the regression lines in Fig. 17 have units of time and can be regarded as a characteristic rise-time of E_{int}. This interpretation is only valid for the Type A events, however, where a single pulse in dE/dt is uniquely associated with the fast-transition in E_{int}. For the 45 Type A events, this characteristic rise time is about 160 ns which is about twice the 83 ns obtained by Willett and Krider (2000, Fig. 5), who plotted just the amplitude of the fast-transition (which they termed E_f) as a function of the peak dE/dt for 76 first strokes in the same dataset with "single dE/dt peaks during the fast-rising portion" (roughly our Type A and Type C). (Willett and Krider (2000) also found that the slow front in those 76 events represented about 50% of the total amplitude of E.)

5.3 Energy Spectral Density of dE/dt

Willett et al. (1990, Appendix A and Fig. A1) have described a method for computing the energy spectral density (ESD) of the early portion of return stroke fields from recorded dE/dt signatures. We have used the same method to compare the ESD of 45 Type A and 49 Type B waveforms over a 15 μs interval that includes the onset of the return stroke and peak E (-9 μs to +6 μs). The results are shown in Fig. 18. Note how the presence of multiple peaks near the fast-transition in E (Type B) enhances the average ESD relative to a single, dominant peak (Type A) above about 5 MHz, and it also produces a relative minimum between 2 and 4 MHz. The mean time-interval between the two largest

negative peaks in dE/dt (in the –1 μs to +1 μs interval) in the 49 Type B strokes was 0.31 ± 0.2 μs, and the median was 0.24 μs; the minimum in the spectrum is consistent with this spacing.

5.4 Subsequent Return Strokes

We have examined the dE/dt waveforms produced by the subsequent return strokes in our dataset, i.e., the strokes that come after the first in a flash and that do not appear to initiate new attachments to ground (e.g., Willett et al.,1995), to see if there were multiple pulses in dE/dt during the onset of those strokes. The results are summarized in Table 2 together with our results for the Type A and Type B first strokes. Table 2 shows that a substantial fraction of the subsequent strokes in natural lightning do produce multiple peaks in dE/dt within ± 1 μs of the dominant peak, and that the subsequent strokes preceded by dart-stepped leaders have a greater fraction of multiple peaks in this interval than the first strokes (66 % vs. 37%). Leteinturier et al. (1990, Fig. 5) and Uman et al. (2000, Fig. 4) give examples of multiple pulses in dE/dt during the onset of subsequent strokes in rocket-triggered lightning. In the future, we plan to analyze the fine-structure of the E_{int} waveforms produced by subsequent strokes in more detail.

5.5 Propagation

As we have seen, the dE/dt and E_{int} waveforms radiated by the first return strokes in cloud-to-ocean lightning frequently contain large variations on a time-scale of tens to hundreds of nanoseconds. The waveforms were recorded at ranges of 4 to 40 km and, as we stated in section 2.0, they have not been

corrected for the effects of ground-wave propagation because the propagation paths were almost entirely over ocean water. Krider et al. (1996) have estimated that propagation over a smooth ocean surface will reduce the peak dE/dt and increase the full-width-at-half-maximum (of the negative half-cycle) by about 6% and 11%, respectively, at a range of 10 km, and by 15% and 33%, respectively, at a range of 35 km (see their Table 2). In order to evaluate whether such effects might be present in our dataset, Fig. 19 and 20 show the values of peak dE/dt (range-normalized to 100 km) and the effective width of the sharp peaks in E_{int}, i.e., the time-interval between the dominant negative peak in dE/dt and the peak of the positive overshoot that immediately follows the dominant peak (as in Fig. 15), as a function of range, respectively. Since neither of these Fig. shows any significant range-dependence, we believe that the effects of propagation in this dataset are minimal.

5.6 Physical Interpretation

If there are large variations in dE/dt and E on a time-scale of tens to hundreds of nanoseconds during the onset of first return strokes, then there must also be comparable variations (but perhaps not a strict proportionality) in the channel current, I, and dI/dt at or close to the point(s) where lightning leaders attach to the surface and the electric fields are produced. Large values of dI/dt will be produced whenever there is an abrupt onset (or termination) of any large current that flows during the breakdown of air, in response to a large potential difference. Possible causes include multiple pulses of current in a single channel, such as might be present if the development of the last step of the downward-propagating

leader or the upward-propagating connecting discharge develops in an intermittent fashion, or if there are large reflections of traveling waves of current during the attachment process. It is also possible that there are multiple channels, perhaps due to branches or forks in the last leader step and/or the upward connecting discharge, or that loops or forks form at the time of attachment. In any case, our results clearly show that the electromagnetic environment near the point(s) where lightning leaders attach to the surface is often more complicated than what would be produced by a single current pulse propagating up a single channel at the time of onset. (see, for example, Rakov and Uman, 1998; 2003, Chapter 12; and Cooray et al., 2004).

6.0 SUMMARY

A re-analysis of the dE/dt and E fields radiated by first return strokes in cloud-to-ocean lightning has shown that there is considerable fine-structure in these waveforms on a time-scale of tens to hundreds of nanoseconds. The dE/dt waveforms can be broadly classified into Type A (35%) that contain a single, dominant (negative) peak in a 5 μs interval that includes the peak E, Type B (37%) that have one or more additional pulses (not counting the dominant peak) within ±1 μs of the dominant peak, and Type C (28%) that have at least one additional pulse in a 3 μs interval (-4 μs to -1 μs) plus the dominant peak, and no additional pulses within ±1 μs of the dominant peak. Integrated dE/dt records show that the corresponding E_{int} signatures have considerable fine-structure that is not resolved by a E digitizer sampling at 10 MHz. This structure includes fast

pulses near the beginning of the slow front, large peaks and shoulders within the slow front and during the fast-transition, and very narrow peaks in E_{int}.

ACKNOWLEDGEMENTS

The first author (NDM) has submitted this research in partial fulfillment of the requirements for a M.S. degree in atmospheric sciences at The University of Arizona. We would like to thank Dr. Charles D. Weidman for guidance during the initial stages of this project. This research has been supported in part by the NASA Kennedy Space Center under grants NAG 10-286, NAG 10-302, and Contract CC-90796B.

REFERENCES

Bailey, J. C., and J. C. Willett, 1989. Catalog of absolutely calibrated, range normalized, wide-band, electric field waveforms from located lightning flashes in Florida: July 24, Aug. 14, 1985 data, U.S. Naval Res. Lab., Washington, DC, NRL Memo Rep. 6497.

Cooray, V., and Y. Ming, 1994. Propagation effects on the lightning – generated electromagnetic fields for homogenous and mixed sea-land paths, J. Geophys. Res.,99, 10, 641 – 652. correction: J. Geophys. Res.,104, 12,227, 1999.

Cooray, V., 2003. Chapter 7 in "The Lightning Flash", edited by V. Cooray, IEE Press, London, 608 pp.

Cooray, V., M. Fernando, and V. Rakov, 2004. A model to represent negative and positive lightning first strokes with connecting leaders, J. Electrostat., 60, 97 – 109.

Cummins, K. L., M. J. Murphy, E. A. Bardo, W. L.Hiscox, R. P. Pyle, and A. E. Pifer, 1998a. A combined TOA/MDF technology upgrade of the U.S. National Lightning Detection Network, J. Geophys. Res., 103, 9035 – 9044.

Cummins, K. L., E. P. Krider, and M. D. Malone, 1998b. The US National Lightning Detection Network and applications of cloud-to-ground lightning data by electric power utilities, IEEE Trans. Electromagn. Compat., 40,465-480.

Izumi, Y., and J. C. Willett, 1991. Catalog of absolutely calibrated, range normalized, wide-band, electric field waveforms from located lightning flashes in Florida – Volume II: Aug. 8, 10 data, Hanscom AFB, MA, Environmental Res. Papers 1082, PL-TR-91-2076.

Krider, E. P., C. D. Weidman, and R. C. Noggle, 1977. Electric-fields produced by lightning stepped leaders, J. Geophys. Res., 82, 951 – 960.

Krider, E. P, R. C. Noggle, A. E. Pifer, and D. L. Vance, 1980. Lightning direction-finding systems for forest fire detection, Bull. Amer. Meteor. Soc., 61, 980 – 986.

Krider, E. P., C. Leteinturier, and J. C. Willett, 1996. Submicrosecond fields radiated during the onset of first return strokes in cloud-to-ground lightning, J. Geophys. Res., 101, 1589-1597.

Leteinturier, C., C. Weidman, J. Hamelin, 1990. Current and electric field derivatives in triggered lightning return strokes, J. Geophys. Res., 95, 811-828.

Maier, M. W., and W. Jafferis, 1985. Locating rocket triggered lightning using LLP lightning locating system at the NASA Kennedy Space Center, in Proceedings of the 10th International Aerospace and Ground Conference on Lightning and Static Electricity (ICOLSE), pp. 337-345, Les ditions de Phys., Les Ulis, France.

Rakov, V. A. and M. A. Uman, 1998. Review and evaluation of lightning return stroke models including some aspects of their applications, IEEE Trans. Electromagn. Compat., 40, 403 – 426.

Rakov, V. A. and M. A. Uman, 2003. Lightning Physics and Effects, Cambridge University Press, Cambridge, pp. 686.

Uman, M. A., V. A. Rakov, G. H. Schnetzer, K. J. Rambo, D. E. Crawford, R. J. Fisher, 2000. Time derivative of the electric field 10, 14, and 30 m from triggered lightning strokes, J. Geophys. Res., 105, 15 577 – 595.

Weidman, C. D. and E. P. Krider, 1978. Fine structure of lightning return stroke wave forms, J. Geophys. Res., 83, 6239-6347, 1978. Correction J. Geophys. Res., 87, 7351, 1982.

Weidman, C. D. and E. P. Krider, 1980. Submicrosecond risetimes in lightning return-stroke fields, Geophys. Res. Lett., 7, 955-958.

Weidman, C. D. and E. P. Krider, 1984. Submikrosekundenstruktur electomagnetischer Blitzfelder, Elektrotechnishe-Zeitschrift-ETZ, 105, 18 – 24.

Weidman, C., J. Hamelin, C. Leteinturier, and L. Nicot, 1986. Correlated current-derivative (dI/dt) and electric field derivative (dE/dt) emitted by triggered lightning, paper presented at the International Aerospace and Ground Conference on Lightning and Static Electricity (ICOLSE), Natl. Interagency Coord. Group, Natl. Atmos. Electr. Ahzards Prot. Agency, Dayton, Ohio.

Willett, J. C., V. P. Idone, R. E. Orville, C. Leteinturier, A. Eybert-Berard, L. Barret, and E. P. Krider, 1988. An experimental test of the “Transmission-Line Model” of electromagnetic radiation from triggered lightning return strokes, J. Geophys. Res., 93, 3867 – 3878.

Willett, J. C., J. C. Bailey, and E. P. Krider, 1989. A class of unusual lightning electric field waveforms with very strong high-frequency radiation, J. Geophys. Res., 94, 16 255-16 267.

Willett, J. C., J. C. Bailey, C. Leteinturier, and E. P. Krider, 1990. Lightning electromagnetic radiation field spectra in the interval from 0.2 to 20 MHz, J. Geophys. Res., 95, 20 367 - 387.

Willett, J. C., D. M. Le Vine, and V. P. Idone, 1995. Lightning-channel morphology revealed by return-stroke radiation field waveforms, J. Geophys. Res., 100, 2727-2738.

Willett, J. C., E. P. Krider, and C. Leteinturier, 1998. Submicrosecond field variations during the onset of first return strokes in cloud-to-ground lightning, J. Geophys. Res., 103, 9027-9034.

Willett, J. C. and E. P. Krider, 2000. Rise times of impulsive high-current processes in cloud-to-ground lightning, IEEE Trans. Anten. Prop., 48, 1442-1451.

Table Captions

Table 1. Values of peak E obtained with the 10 MHz digitizer and peak E_{int} (range-normalized to 100 km) for Type A, B, and C first return strokes.

Table 2. Number and types of return strokes that have multiple pulses in dE/dt during the onset of the stroke.

Figure Captions

Fig. 1 (a) The “classical” dE/dt and E waveforms radiated by a first return stroke (Type A). (b) The same waveforms as in (a) on an expanded time scale. The integrated dE/dt waveform or E_{int} is shown in red, and the asterisks denote individual samples of E obtained with the 10 MHz digitizer. The day number and time of the event (UT) are given at the top of the plot, and the range is shown in the upper right corner.

Fig. 2. A waveform that contained multiple pulses in dE/dt near the peak E (Type B). See also caption for Fig. 1.

Fig. 3. Summary of the dE/dt pulses that met our amplitude criteria in the –9 μs to +1 μs time interval (relative to the time of the dominant peak) for all 131 first stroke waveforms in our dataset. (a) The numbers of pulses (not counting the dominant peak) in consecutive 1 μs bins; (b) the average amplitude of these pulses relative to the corresponding dominant peaks; and (c) an example that illustrates the types of pulses that were counted in (a) and averaged in (b). The dashed horizontal line in (c) shows a threshold level that was 10% of the dominant peak, D. The pulses marked P1 and P2 met our selection criteria and were counted.

Fig. 4. A Type B waveform with two γ-shoulders near the fast-transition in E_{int}. The horizontal green line in the lower panel shows the corrected zero level used to measure the values of peak E_{int}.

Fig. 5. A Type B waveform with a γ-shoulder during the fast-transition of E_{int}.

Fig. 6. A Type B waveform that has two γ-peaks prior to the peak E_{int}. Note that the time of the dominant peak in dE/dt precedes the peak E_{int} by 0.5 μs.

Fig. 7. A complex Type B waveform that has several large pulses in dE/dt during the development of the slow front.

Fig. 8. A Type C waveform that have leader step (LS) and leader burst (LB) impulses near the beginning of the slow front.

Fig. 9. A Type C waveform that containes a well-defined γ-peak during the development of the slow front.

Fig. 10. A Type C waveform that has a convex slow front.

Fig. 11. A Type C waveform that contains a large fast-rising shoulder near the beginning of the slow front.

Fig. 12. A Type C waveform that contains a large fast-rising shoulder near the beginning of the slow front.

Fig. 13. A Type A waveform with a very narrow peak in E_{int}. The LS pulse at –5 μs was produced by the last step of the stepped-leader before the return stroke.

Fig. 14. Distribution of the ratios of peak E_{int} to peak E (10 MHz) for all 131 first strokes in our data set. The scale of the cumulative distribution (dashed line) is shown on the right.

Fig. 15. Distribution of the time intervals between the dominant (negative) peak in dE/dt and the peak of the positive overshoot that immediately follows the dominant peak for 114 first strokes where the positive overshoot was well-defined. The scale of the cumulative distribution (dashed line) is shown on the right.

Fig. 16. Distribution of the peak amplitude of the (positive) overshoot in dE/dt relative to the absolute value of the (negative) dominant peak for the same 114 strokes that are shown in Fig. 15. The scale of the cumulative distribution (dashed line) is shown on the right.

Fig. 17. Peak E_{int} vs. the (dominant) peak dE/dt for 45 Type A (red), 49 Type B (green), and 37 Type C (blue) first strokes waveforms.

Fig. 18. The average energy spectral density (ESD) of dE/dt vs. frequency for all 45 Type A (black) and 49 Type B (red) waveforms. The ESD was computed assuming that 0 dB = 1 $(V/m/s/Hz)^2$ at 100 km.

Fig. 19. The peak dE/dt (range-normalized to 100 km) vs. range for all 131 first strokes in our data set.

Fig. 20. The time-intervals between the dominant (negative) peak in dE/dt and the peak of the (positive) overshoot that follows vs. range for the same 114 first strokes that are shown in Fig. 15 and Fig. 16.

Type	No.	Mean peak E and Standard Deviation (V/m)	Median peak E (V/m)	Mean peak E_{int} and Standard Deviation (V/m)	Median peak E_{int} (V/m)
A	45	-7.0 ± 2.9	-6.3	-7.6 ± 2.8	-7.4
B	49	-10.3 ± 5.4	-8.7	-10.7 ± 5.5	-9.0
C	37	-8.3 ± 3.8	-7.1	-8.7 ± 3.7	-7.6
All	131	-8.6 ± 4.4	-7.2	-9.0 ± 4.4	-7.9
B/A Ratio		1.47	1.38	1.40	1.21

TABLE 1

Type of Return Stroke	Total Number	Number with multiple peaks in dE/dt within ±1 μs of the dominant peak (Type B)	Number with multiple peaks in dE/dt within -4 μs to -1 μs (Type C)
First	131	49 (37.4 %)	37 (28 %)
Subsequent with Normal or Chaotic Leader	54	17(31.5 %)	
Subsequent with Dart-Stepped Leader	32	21 (65.6 %)	

TABLE 2

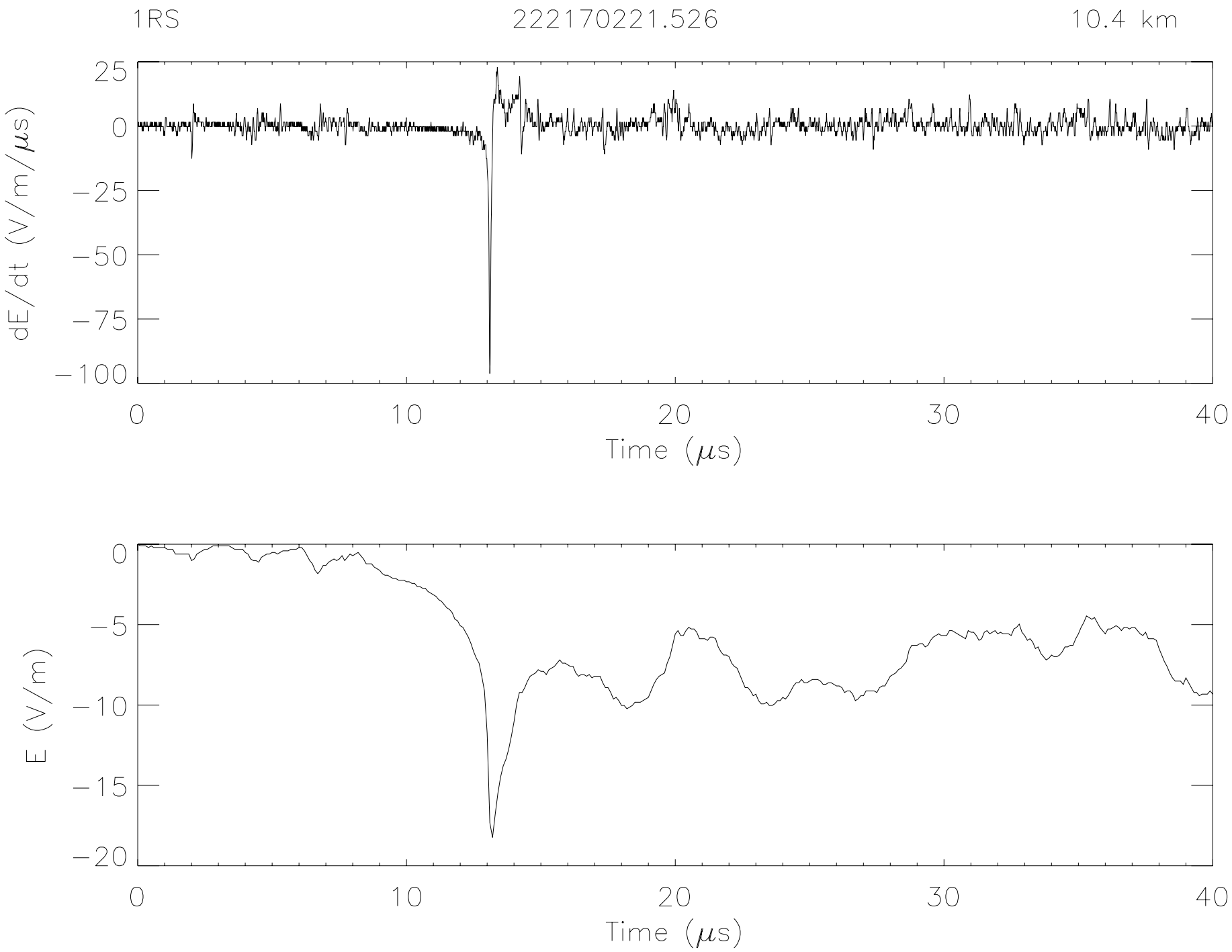
1RS
222170221.526
10.4 km
dE/dt (V/m/μs)
25
0
−25
−50
−75
−100
0
10
20
30
40
Time (μs)
E (V/m)
0
−5
−10
−15
−20
0
10
20
30
40
Time (μs)

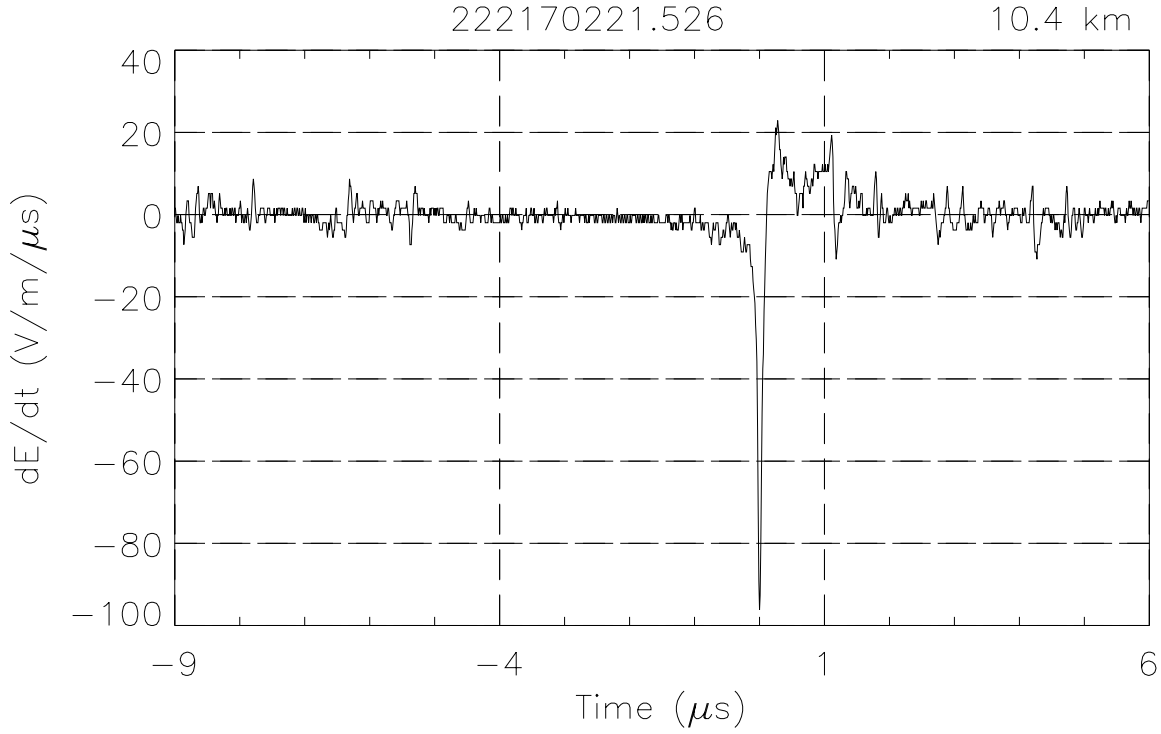
222170221.526
10.4 km
40
20
0
−20
−40
−60
−80
−100
dE/dt (V/m/μs)
−9
−4
1
6
Time (μs)

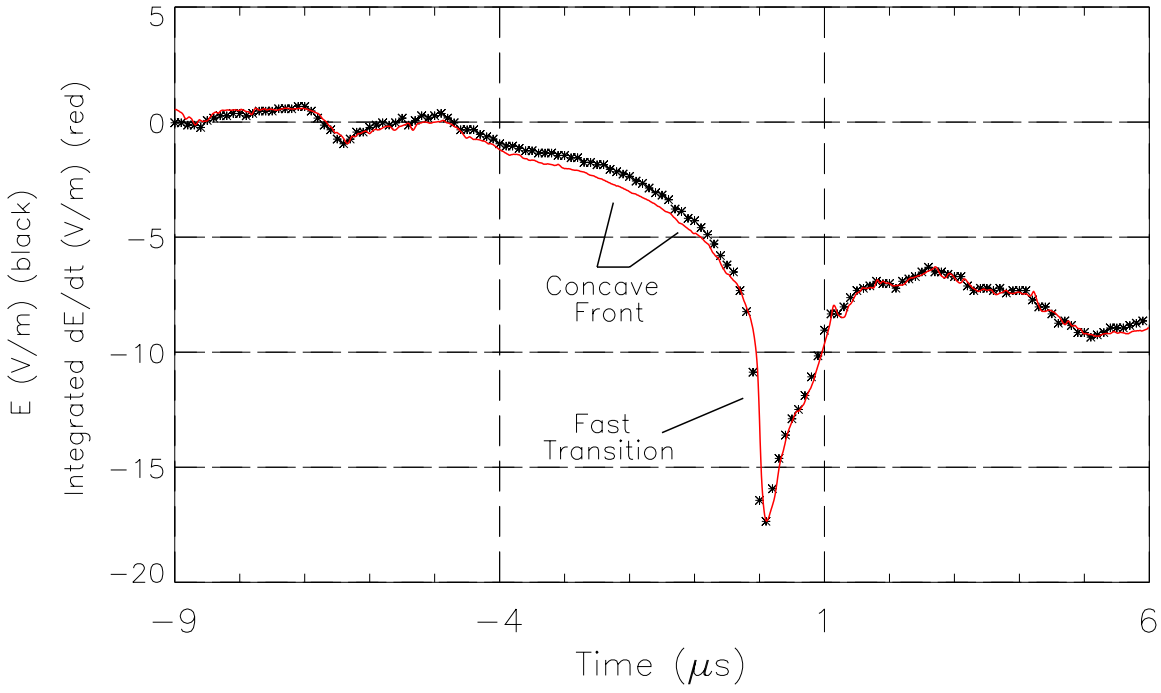
5
0
−5
−10
−15
−20
E (V/m) (black)
Integrated dE/dt (V/m) (red)
Concave
Front
Fast
Transition
−9
−4
1
6
Time (μs)

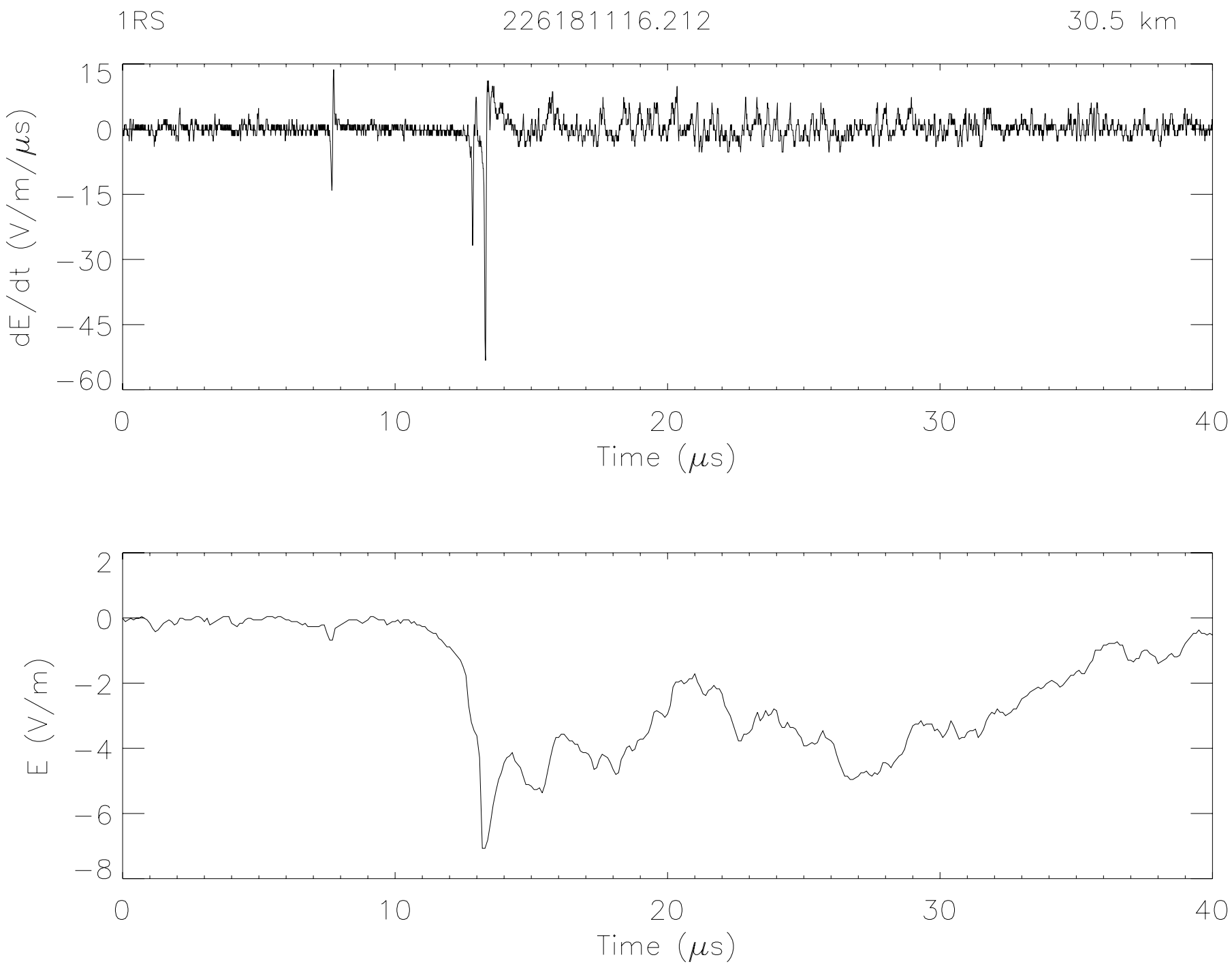
1RS
226181116.212
30.5 km
dE/dt (V/m/μs)
15
0
−15
−30
−45
−60
0
10
20
30
40
Time (μs)
E (V/m)
2
0
−2
−4
−6
−8
0
10
20
30
40
Time (μs)

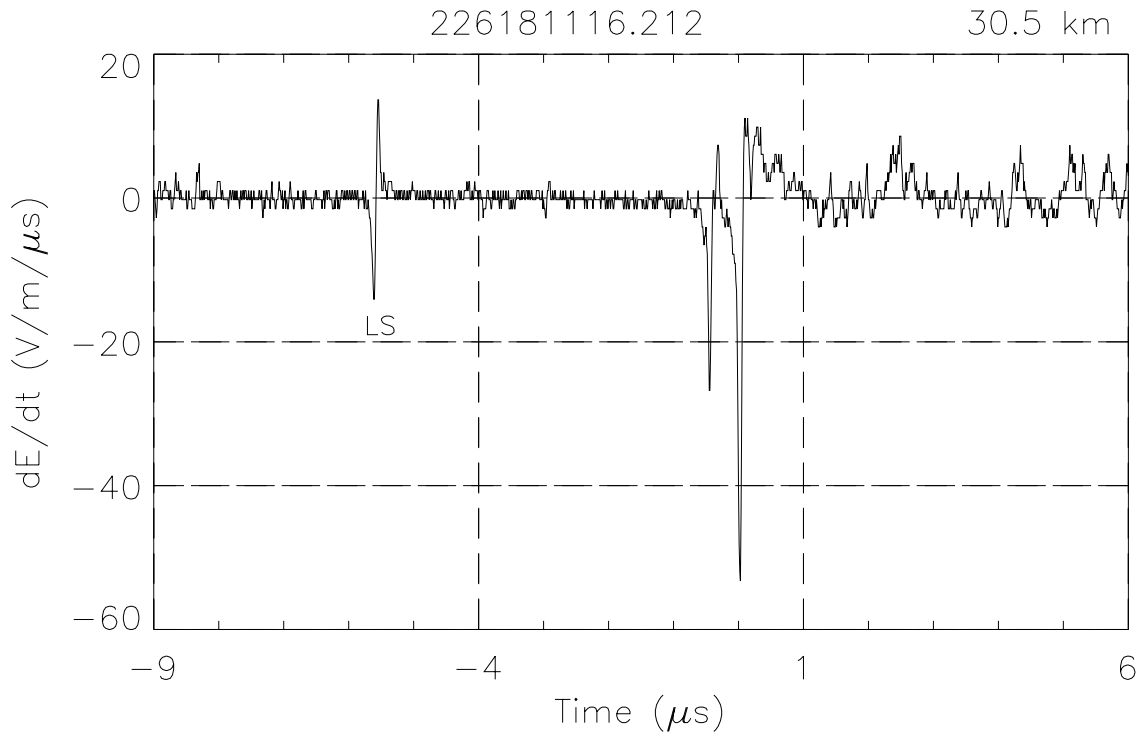
226181116.212
30.5 km
20
0
−20
−40
−60
dE/dt (V/m/μs)
LS
−9
−4
1
6
Time (μs)

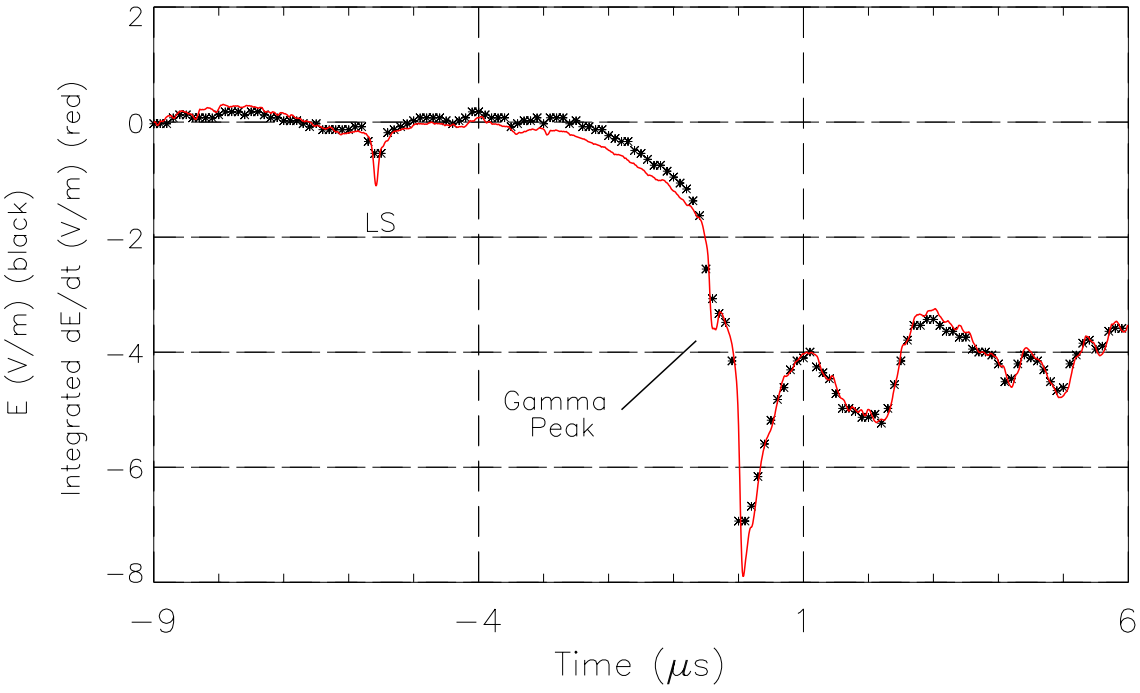
2
0
−2
−4
−6
−8
E (V/m) (black)
Integrated dE/dt (V/m) (red)
LS
Gamma
Peak
−9
−4
1
6
Time (μs)

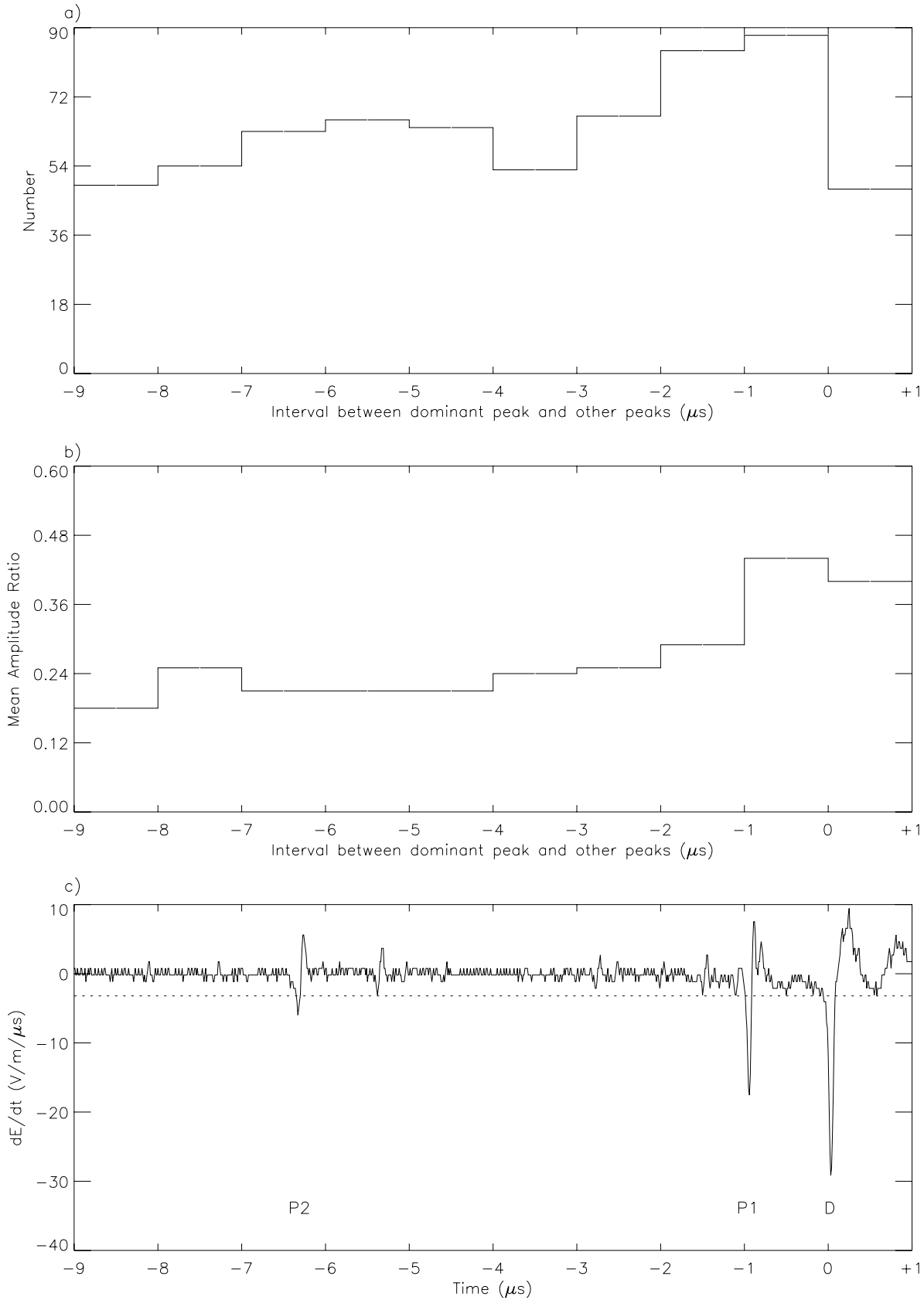
a)
90
72
54
36
18
0
Number
−9
−8
−7
−6
−5
−4
−3
−2
−1
0
+1
Interval between dominant peak and other peaks (μs)
b)
0.60
0.48
0.36
0.24
0.12
0.00
Mean Amplitude Ratio
−9
−8
−7
−6
−5
−4
−3
−2
−1
0
+1
Interval between dominant peak and other peaks (μs)
c)
10
0
−10
−20
−30
−40
dE/dt (V/m/μs)
P2
P1
D
−9
−8
−7
−6
−5
−4
−3
−2
−1
0
+1
Time (μs)

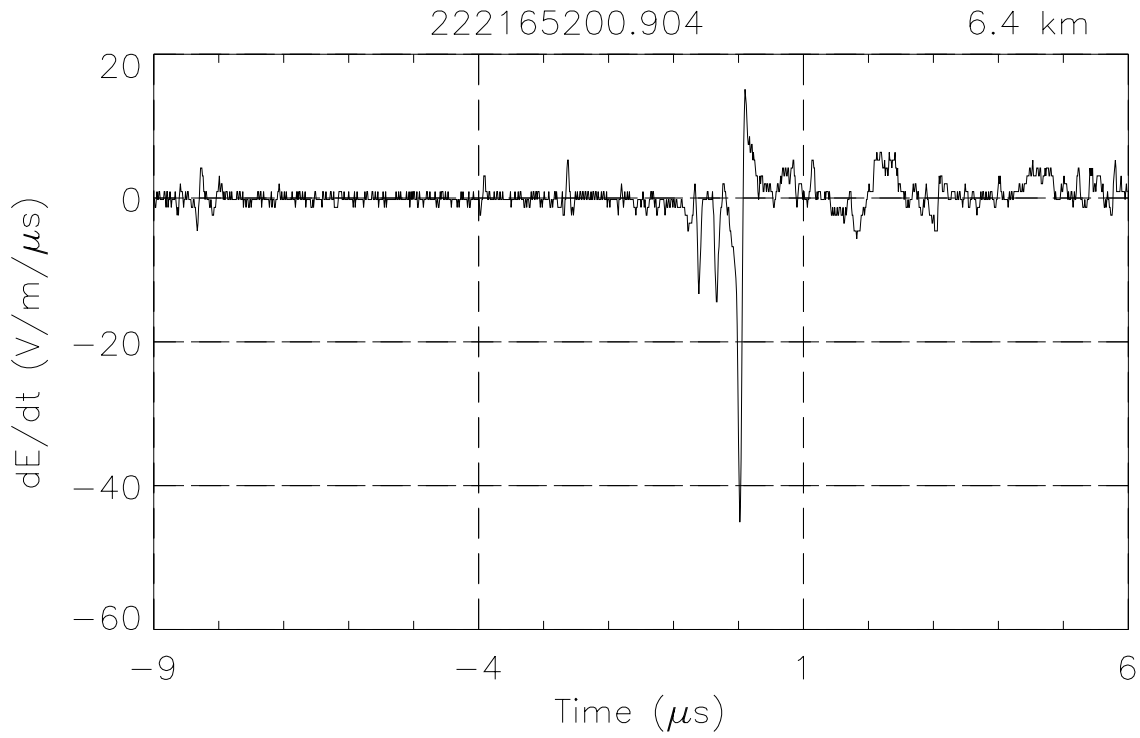
222165200.904
6.4 km
20
0
−20
−40
−60
dE/dt (V/m/μs)
−9
−4
1
6
Time (μs)

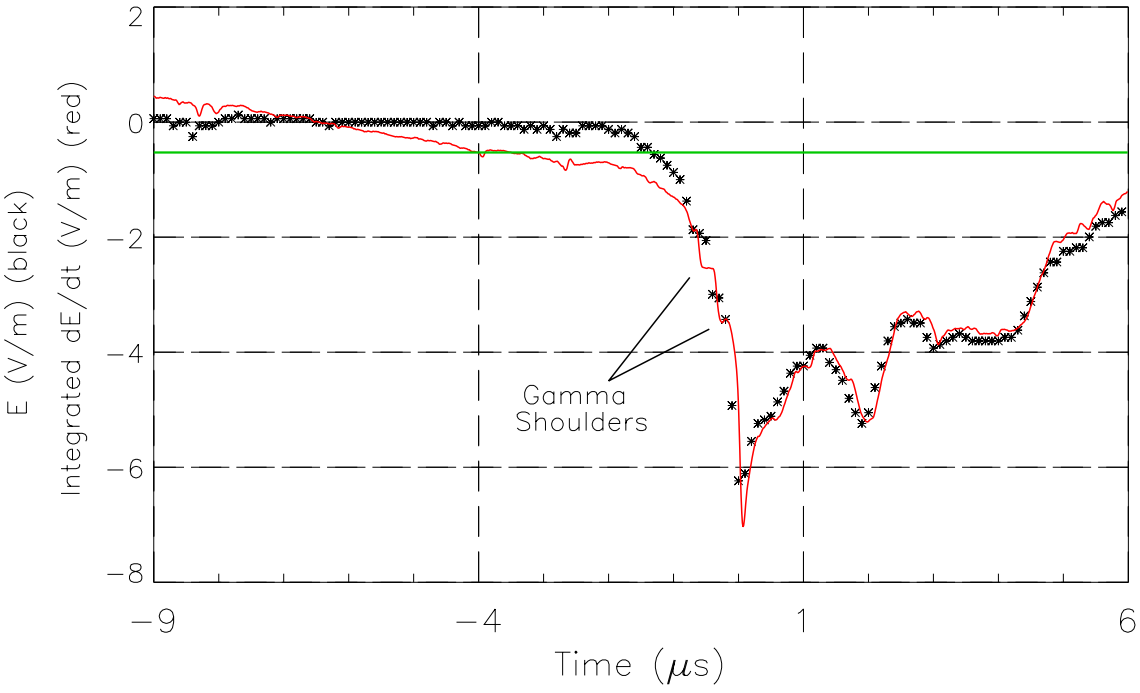
2
0
−2
−4
−6
−8
E (V/m) (black)
Integrated dE/dt (V/m) (red)
Gamma
Shoulders
−9
−4
1
6
Time (μs)

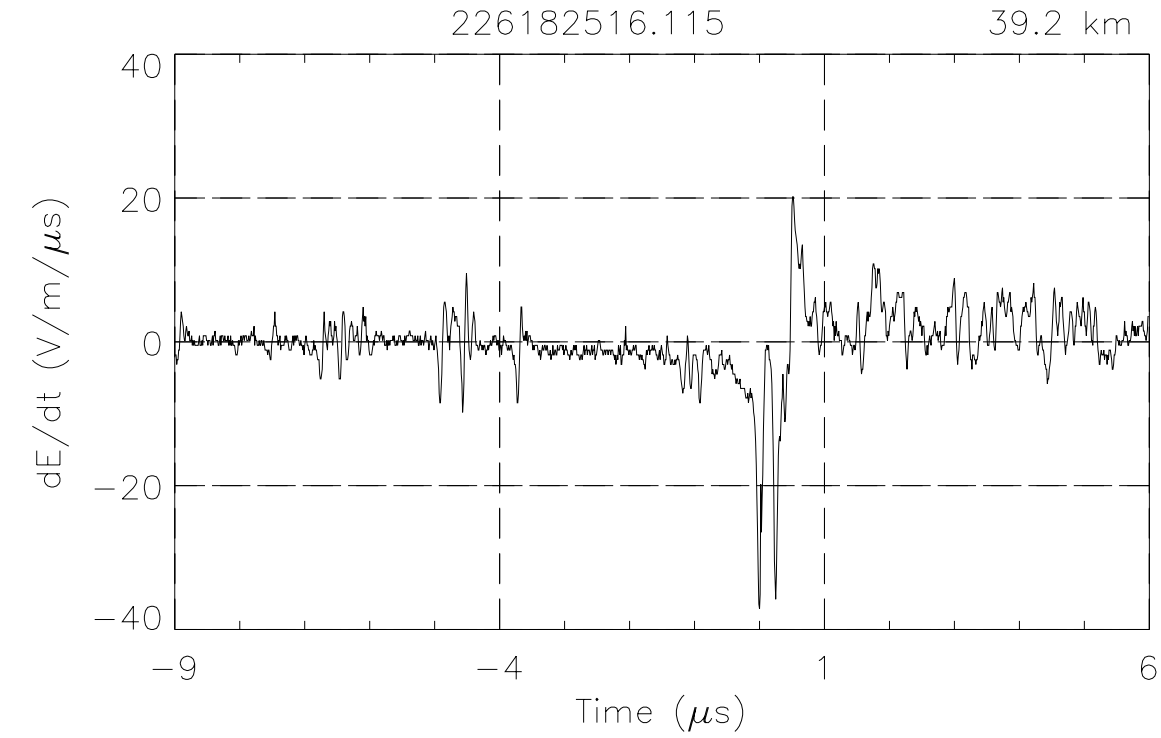
226182516.115
39.2 km
40
20
0
−20
−40
dE/dt (V/m/μs)
−9
−4
1
6
Time (μs)

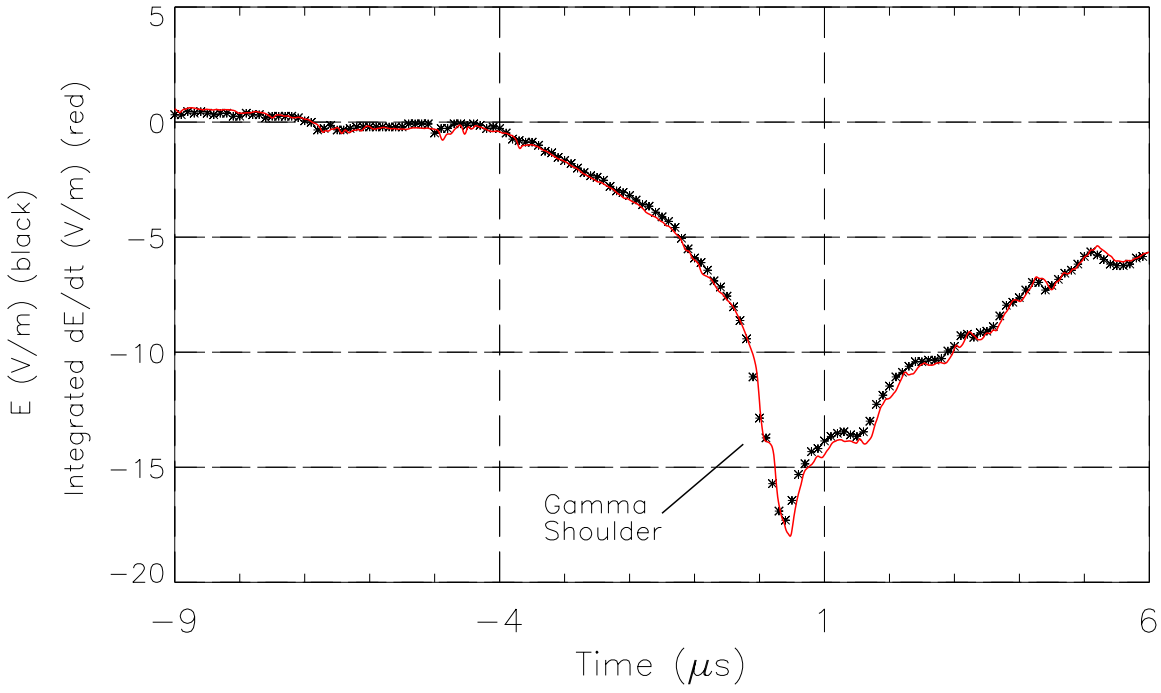
5
0
−5
−10
−15
−20
E (V/m) (black)
Integrated dE/dt (V/m) (red)
Gamma
Shoulder
−9
−4
1
6
Time (μs)

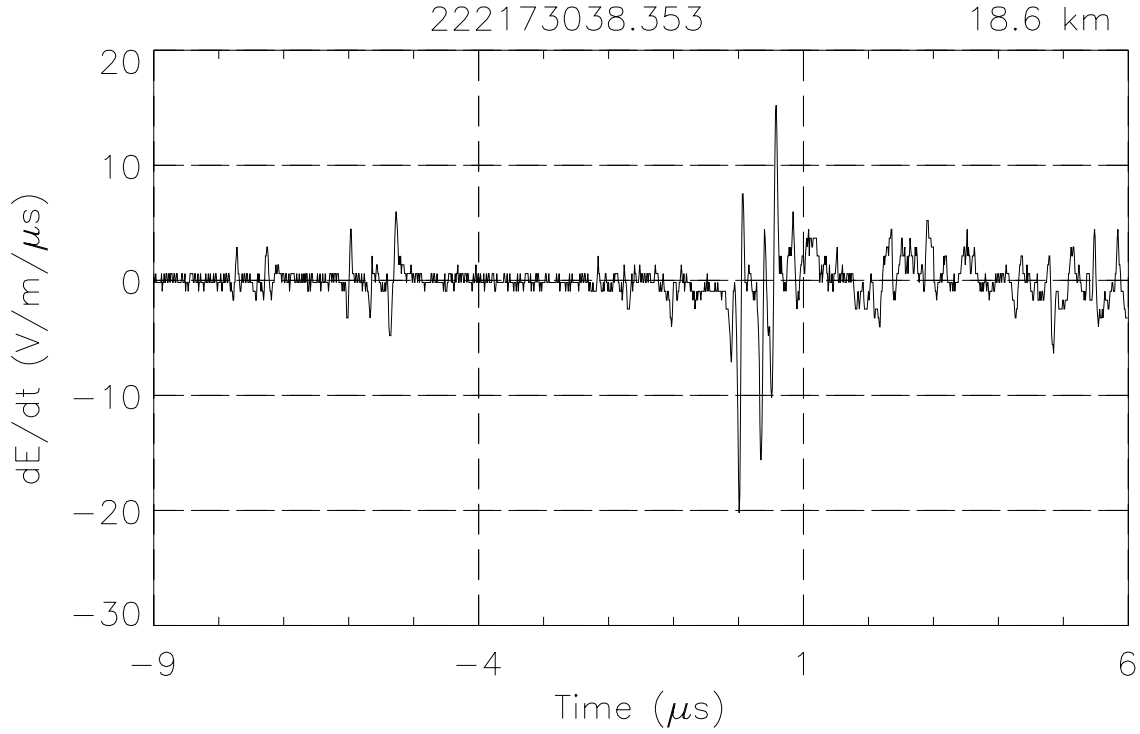
222173038.353
18.6 km
dE/dt (V/m/μs)
20
10
0
−10
−20
−30
−9
−4
1
6
Time (μs)

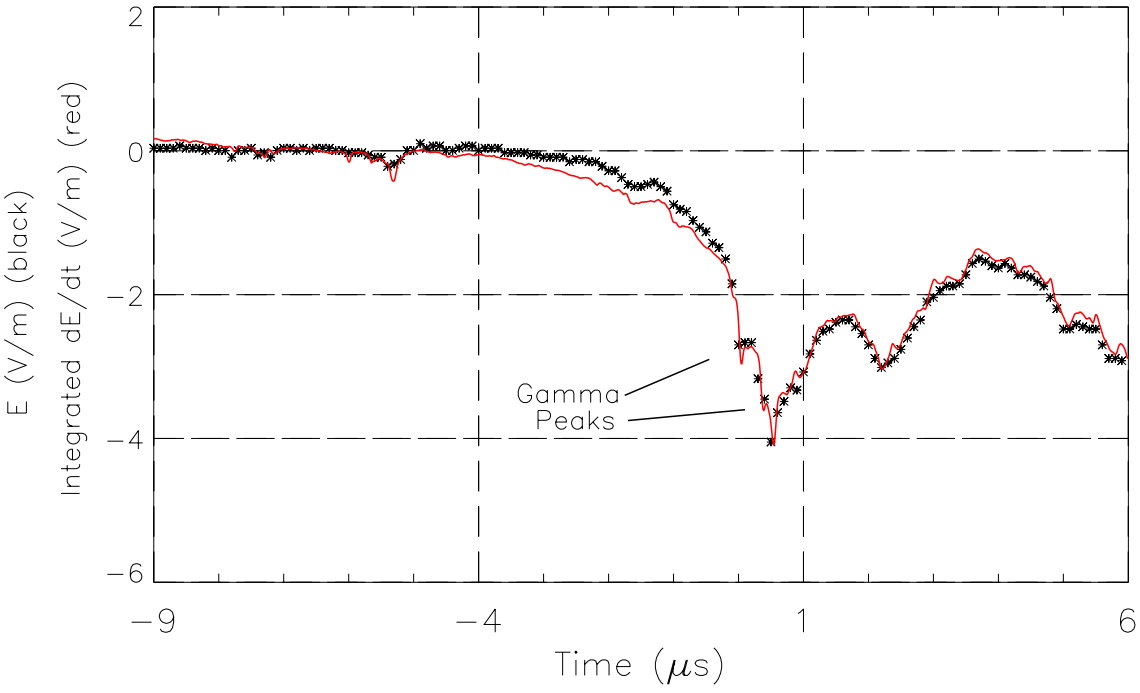
E (V/m) (black)
Integrated dE/dt (V/m) (red)
2
0
−2
−4
−6
Gamma
Peaks
−9
−4
1
6
Time (μs)

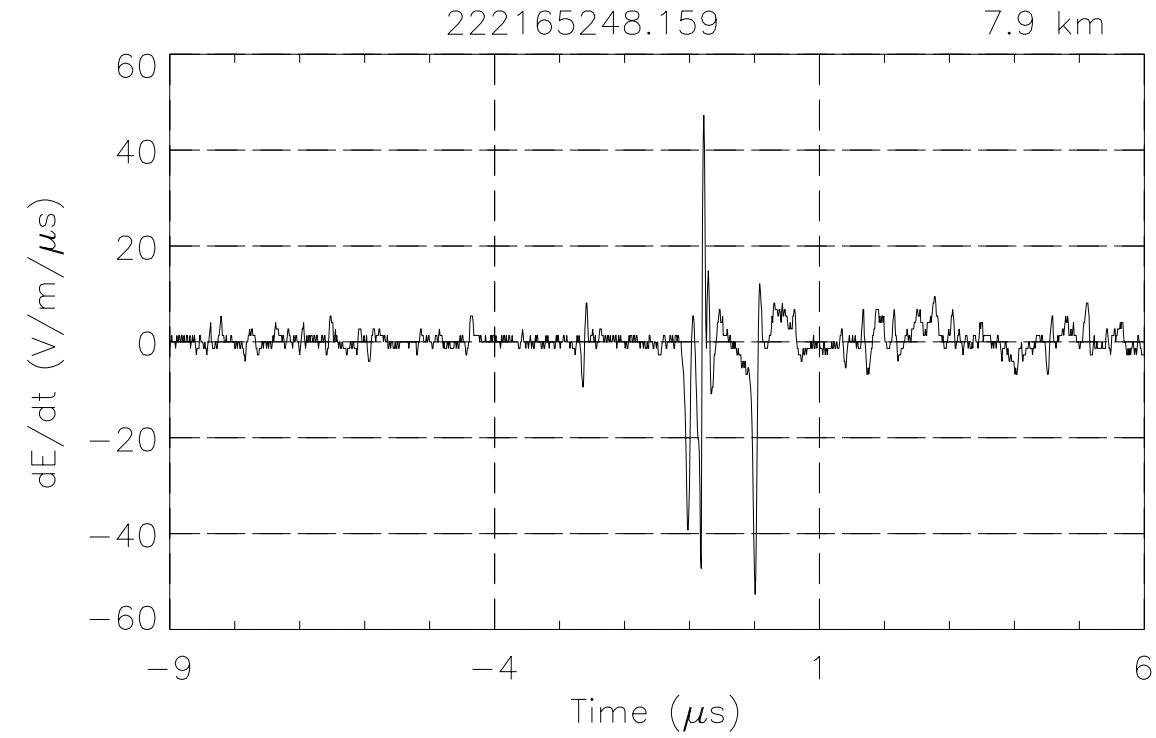
222165248.159
7.9 km
60
40
20
0
−20
−40
−60
dE/dt (V/m/μs)
−9
−4
1
6
Time (μs)

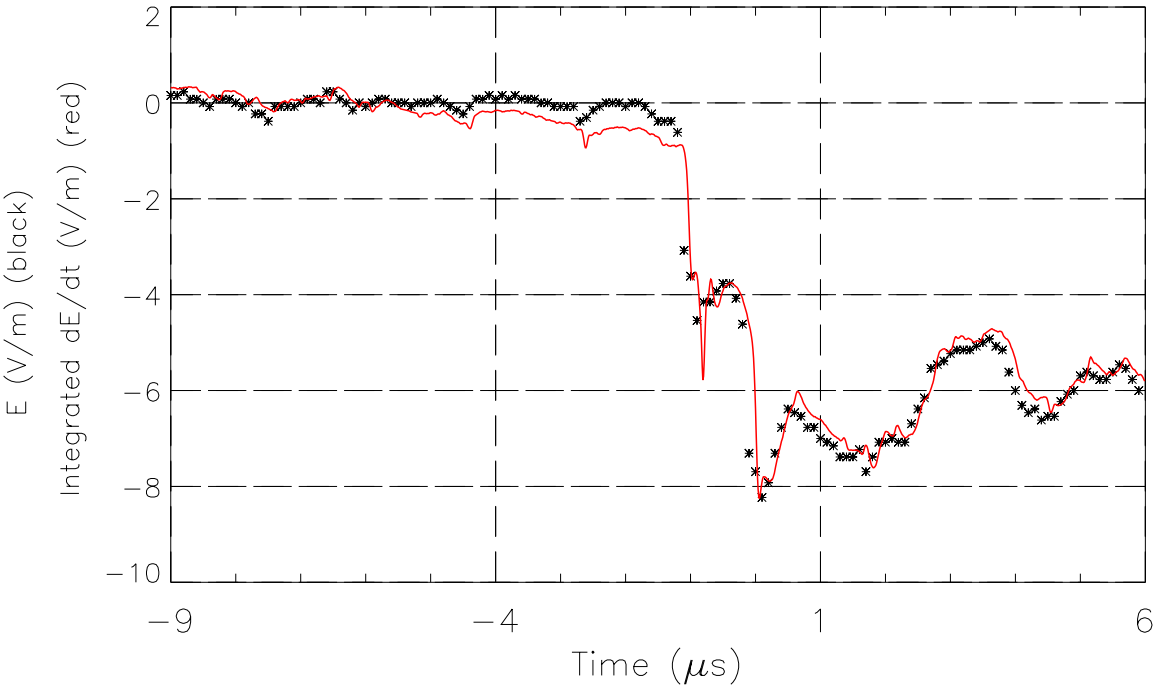
2
0
−2
−4
−6
−8
−10
E (V/m) (black)
Integrated dE/dt (V/m) (red)
−9
−4
1
6
Time (μs)

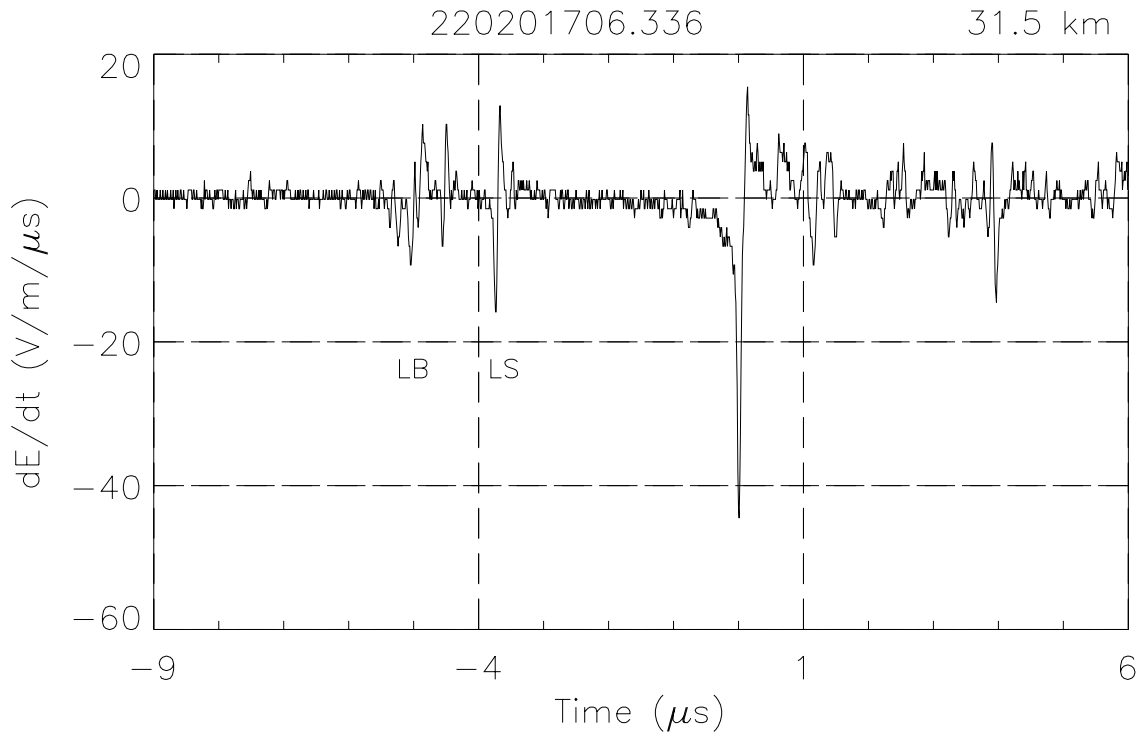
220201706.336
31.5 km
20
0
−20
−40
−60
dE/dt (V/m/μs)
LB
LS
−9
−4
1
6
Time (μs)

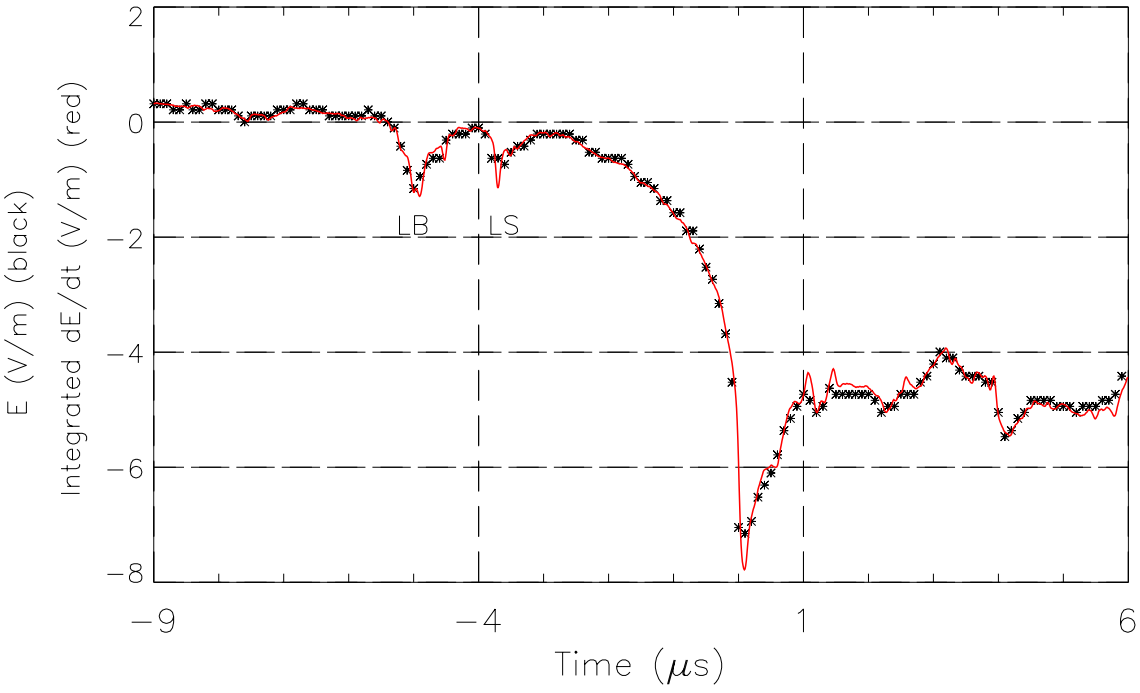
2
0
−2
−4
−6
−8
E (V/m) (black)
Integrated dE/dt (V/m) (red)
LB
LS
−9
−4
1
6
Time (μs)

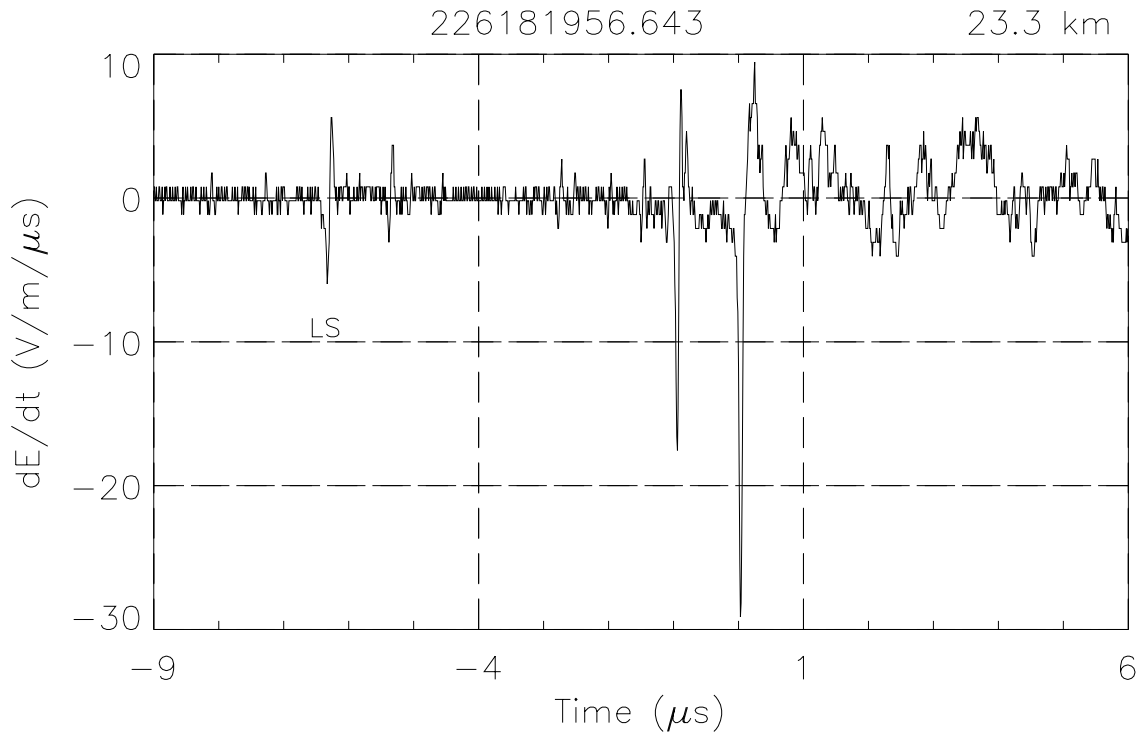
226181956.643
23.3 km
10
0
−10
−20
−30
dE/dt (V/m/μs)
LS
−9
−4
1
6
Time (μs)

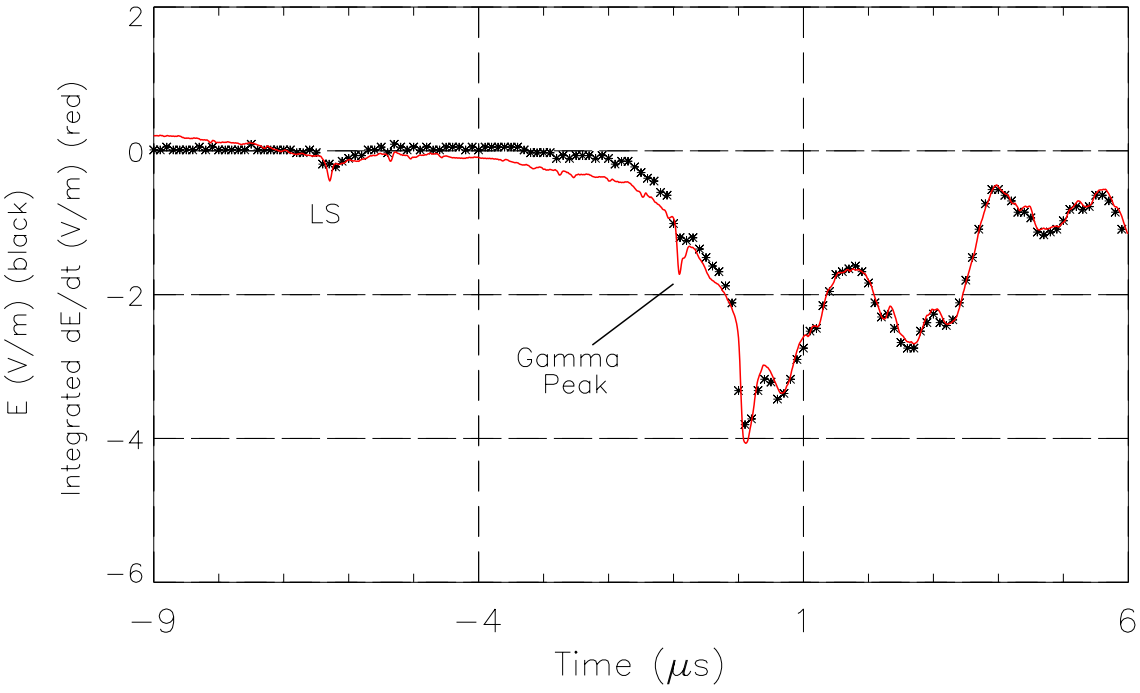
2
0
−2
−4
−6
E (V/m) (black)
Integrated dE/dt (V/m) (red)
LS
Gamma
Peak
−9
−4
1
6
Time (μs)

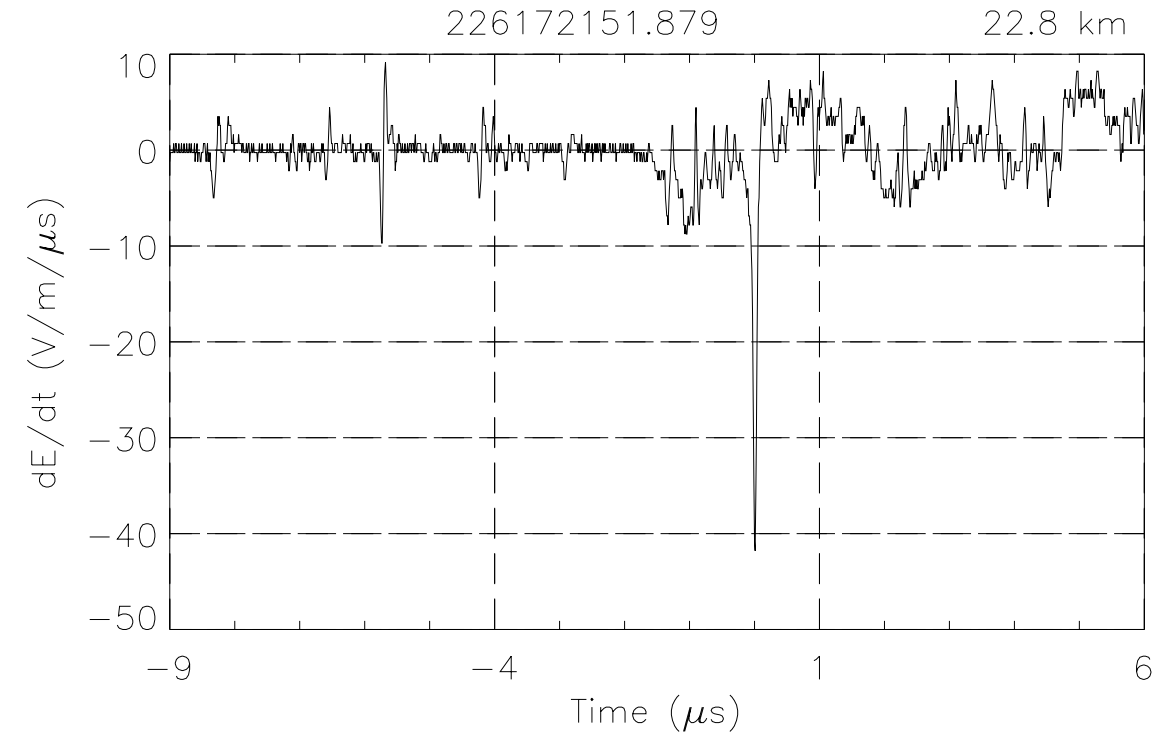
226172151.879
22.8 km
10
0
−10
−20
−30
−40
−50
dE/dt (V/m/μs)
−9
−4
1
6
Time (μs)

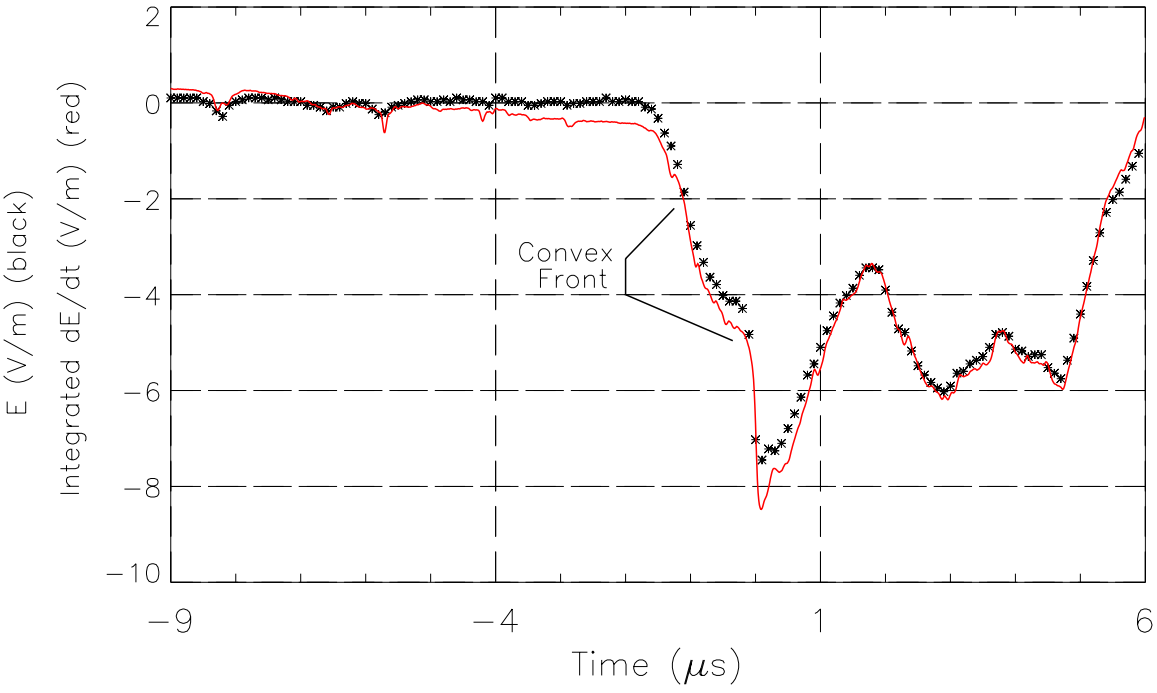
2
0
−2
−4
−6
−8
−10
E (V/m) (black)
Integrated dE/dt (V/m) (red)
Convex
Front
−9
−4
1
6
Time (μs)

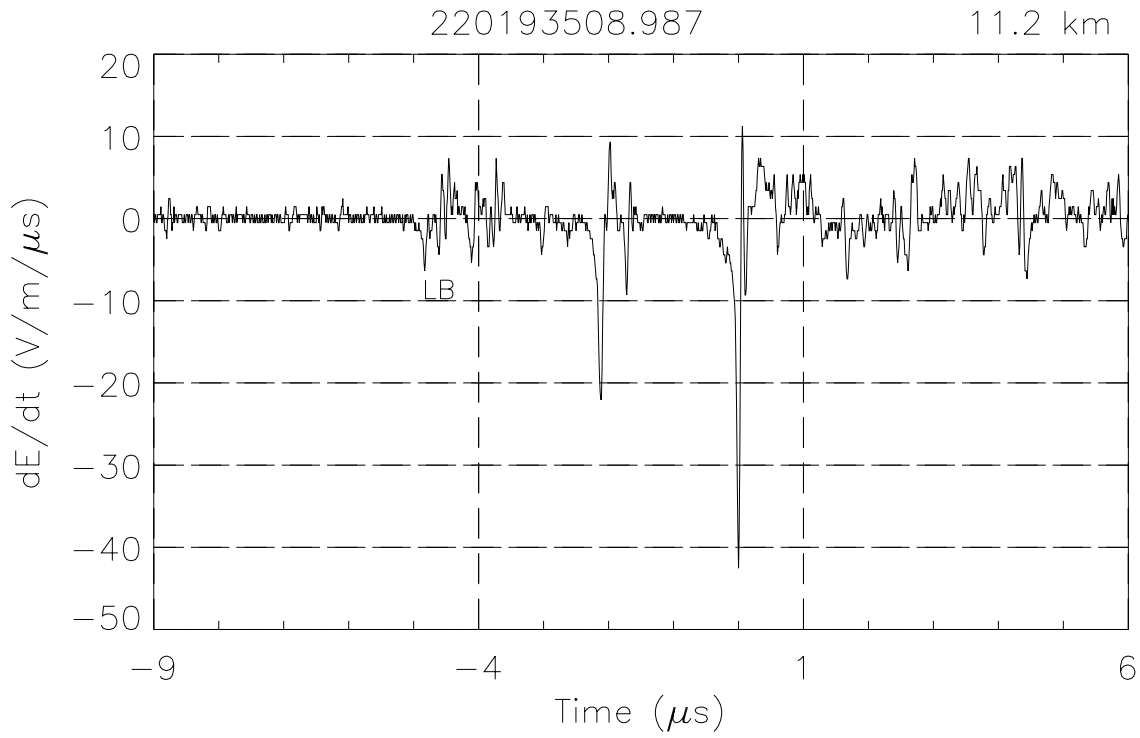
220193508.987
11.2 km
dE/dt (V/m/μs)
20
10
0
−10
−20
−30
−40
−50
LB
−9
−4
1
6
Time (μs)

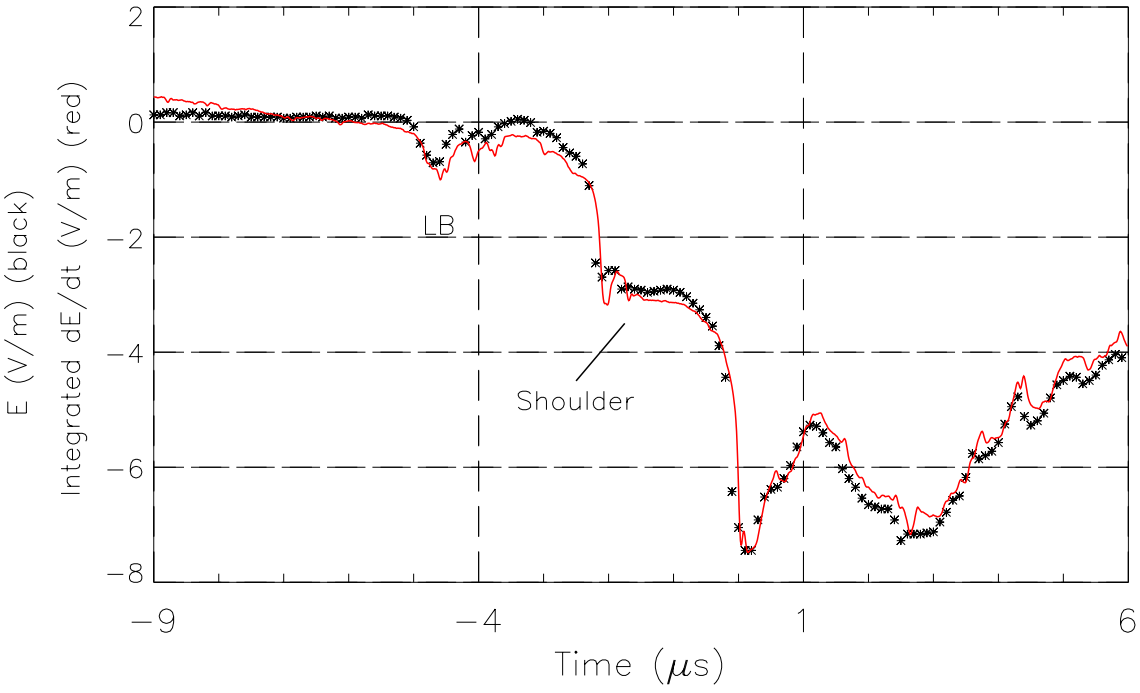
E (V/m) (black)
Integrated dE/dt (V/m) (red)
2
0
−2
−4
−6
−8
LB
Shoulder
−9
−4
1
6
Time (μs)

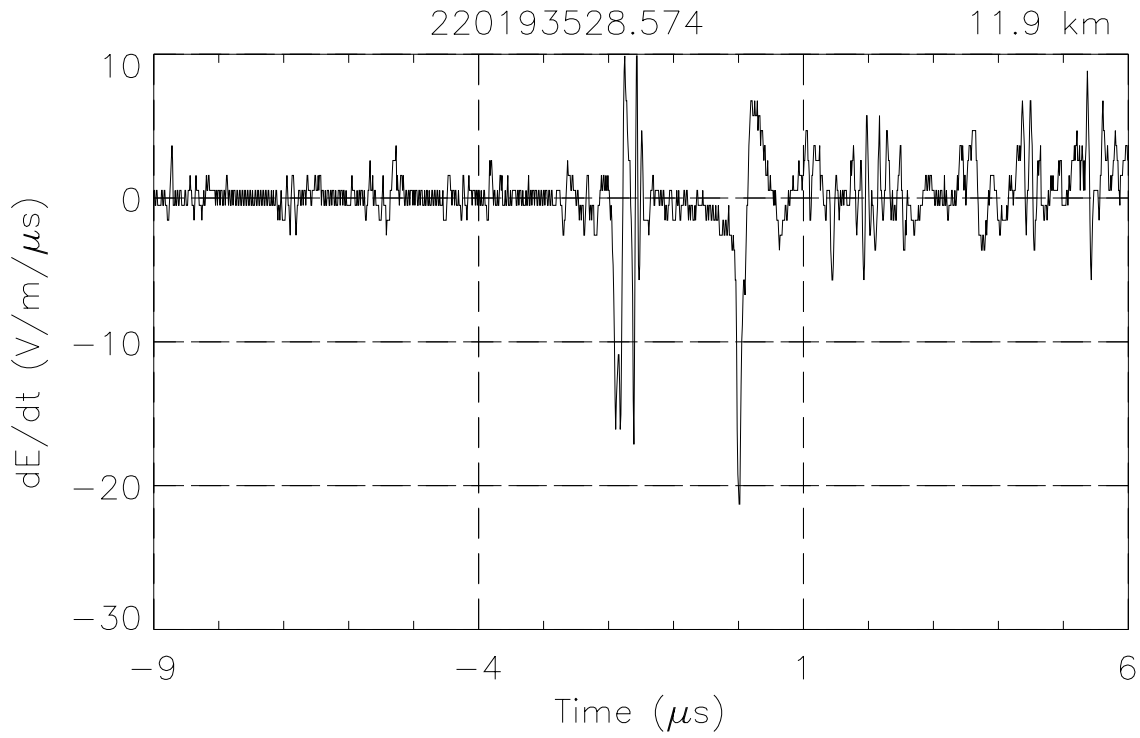
220193528.574
11.9 km
10
0
−10
−20
−30
dE/dt (V/m/μs)
−9
−4
1
6
Time (μs)

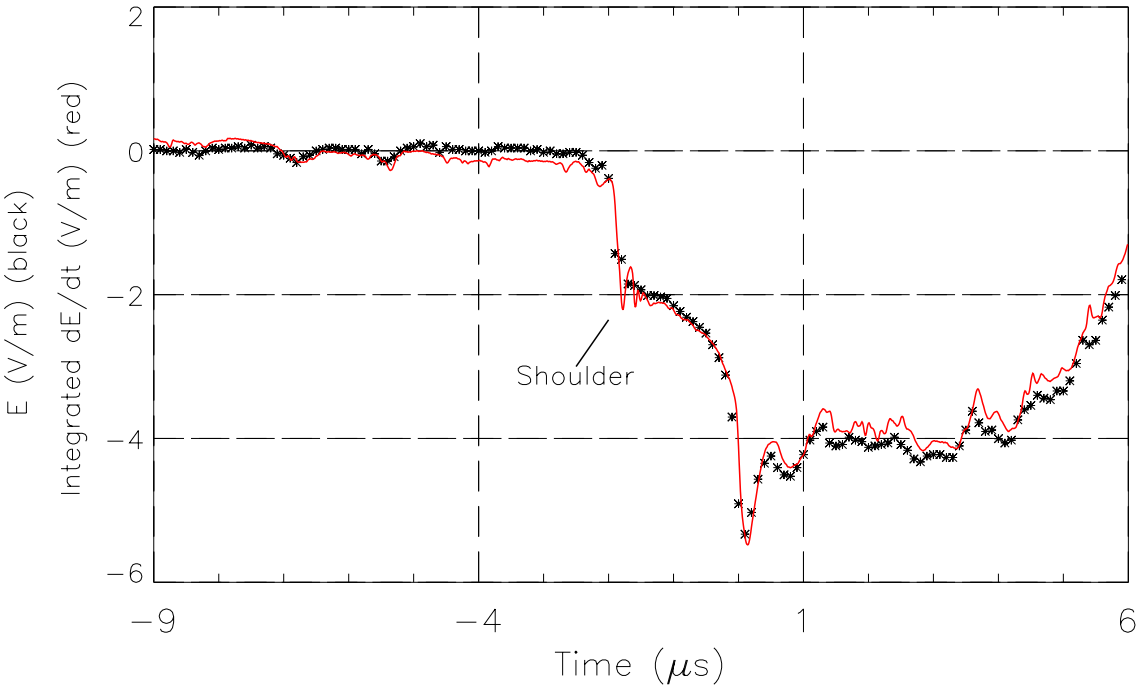
2
0
−2
−4
−6
E (V/m) (black)
Integrated dE/dt (V/m) (red)
Shoulder
−9
−4
1
6
Time (μs)

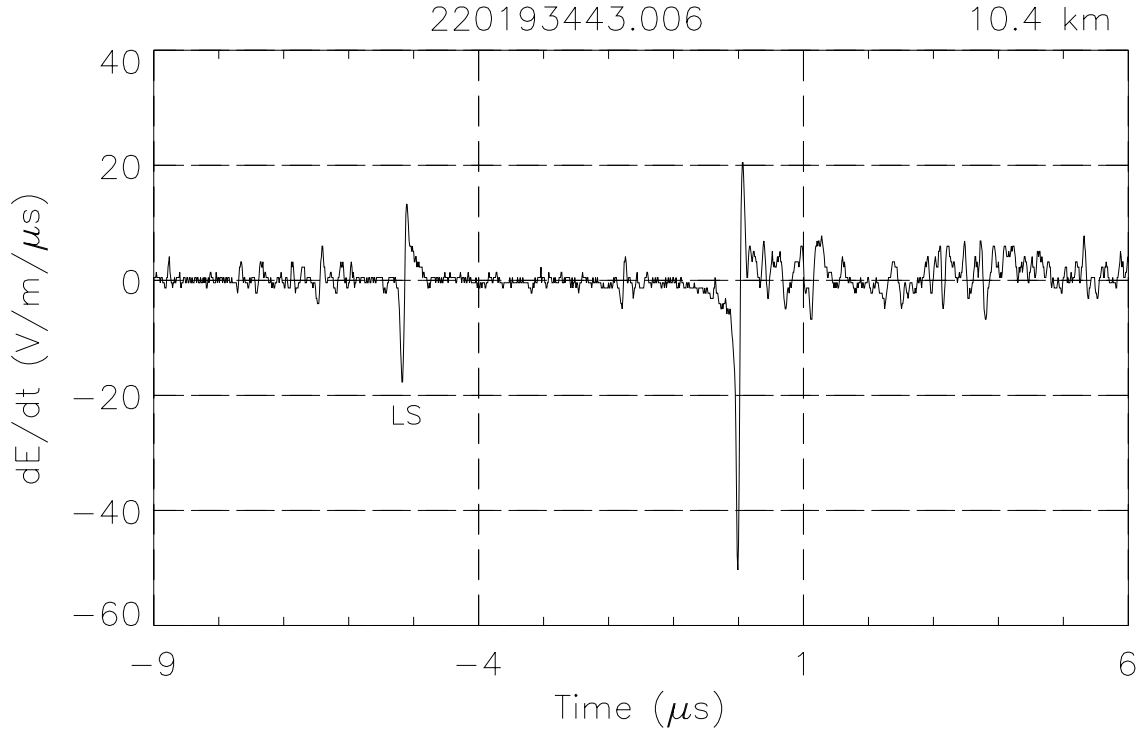
220193443.006
10.4 km
40
20
0
−20
−40
−60
dE/dt (V/m/μs)
LS
−9
−4
1
6
Time (μs)

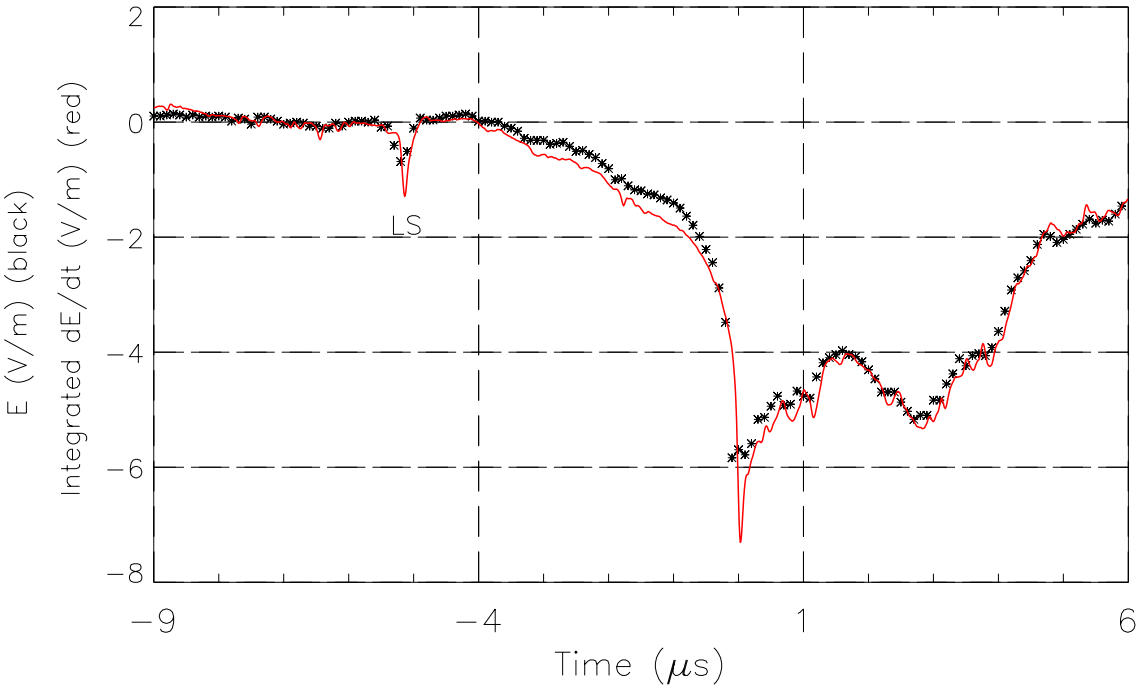
2
0
−2
−4
−6
−8
E (V/m) (black)
Integrated dE/dt (V/m) (red)
LS
−9
−4
1
6
Time (μs)

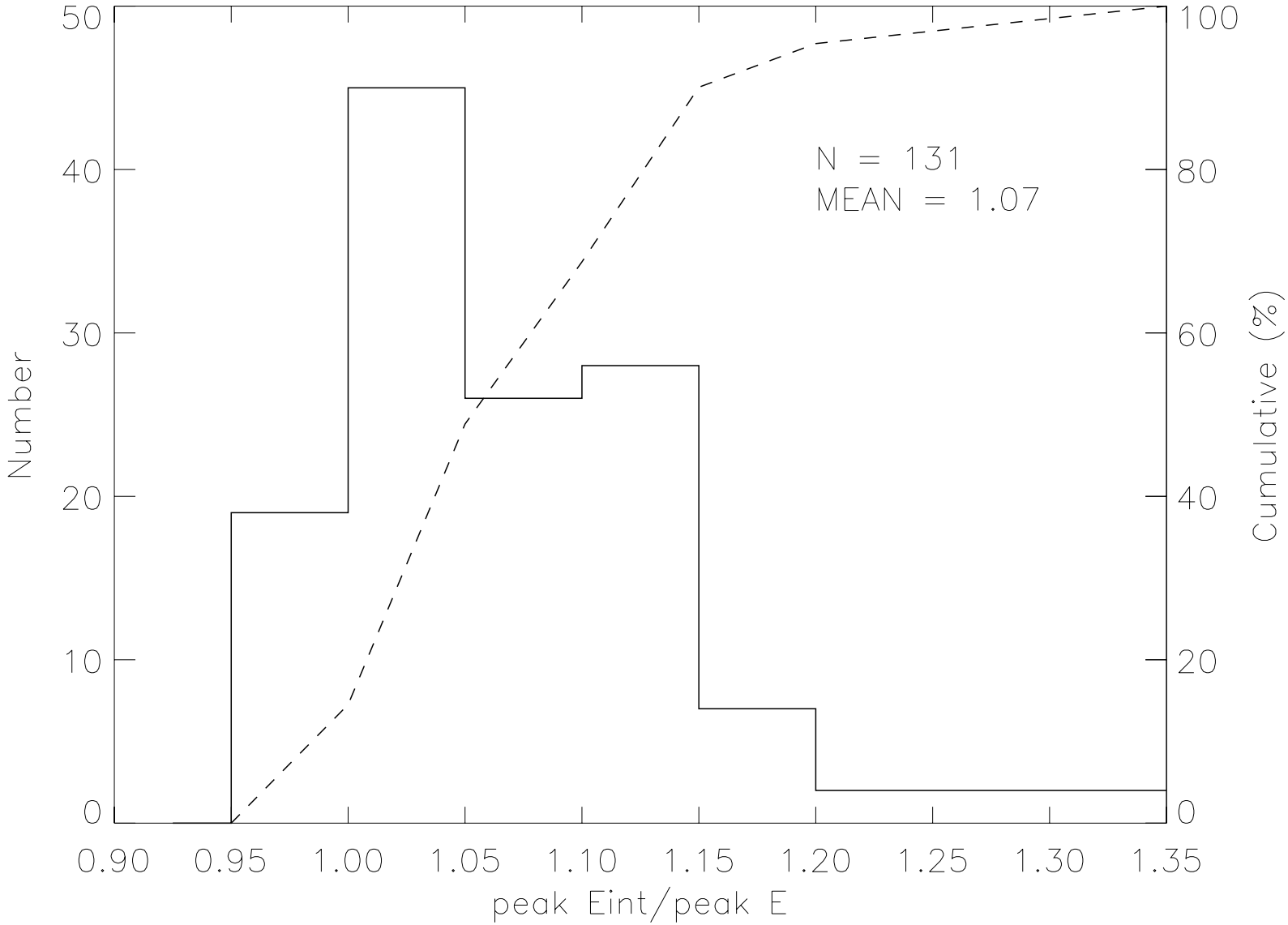
N = 131
MEAN = 1.07
Number
Cumulative (%)
peak Eint/peak E
0
10
20
30
40
50
0
20
40
60
80
100
0.90
0.95
1.00
1.05
1.10
1.15
1.20
1.25
1.30
1.35

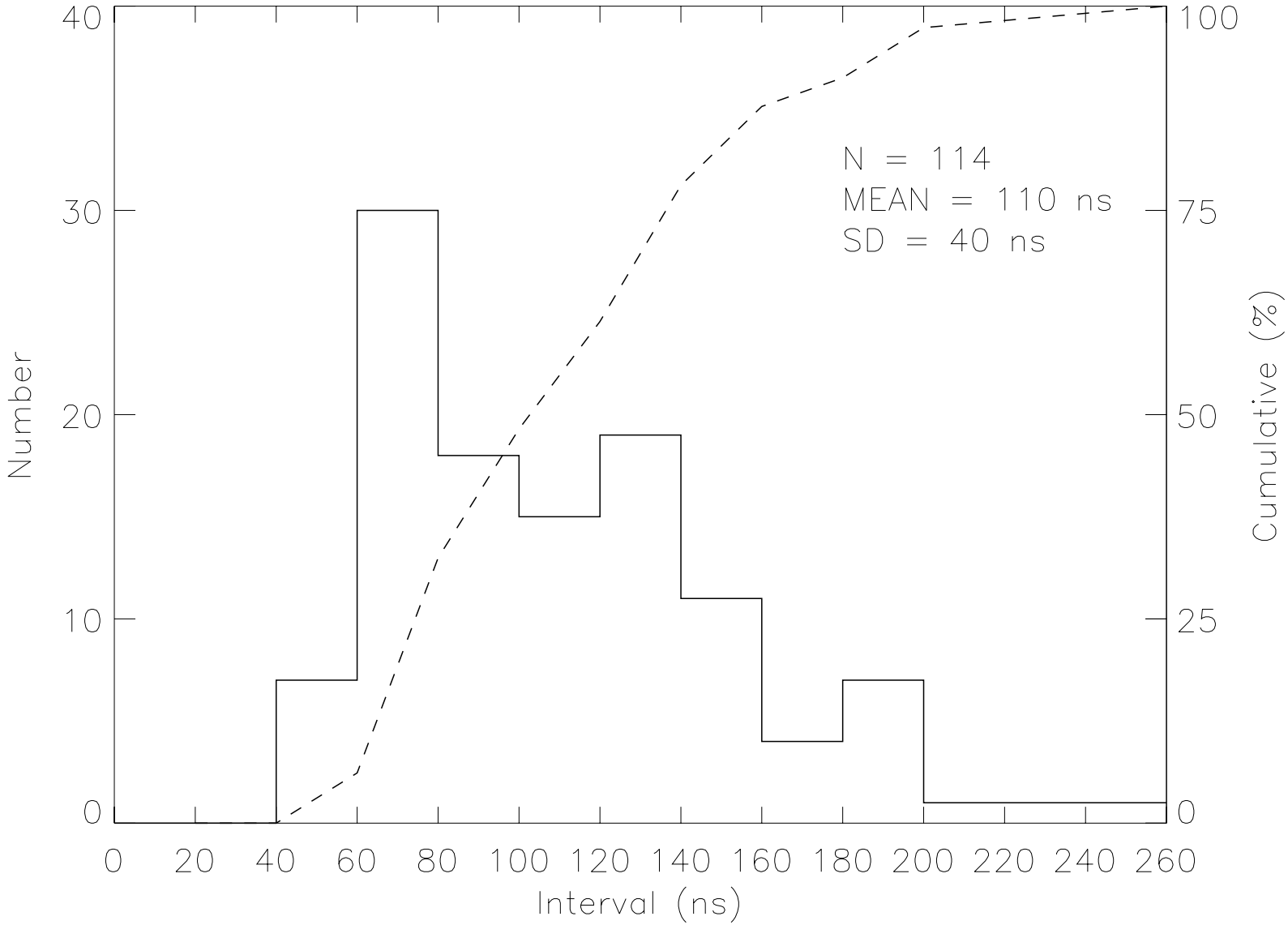
N = 114
MEAN = 110 ns
SD = 40 ns
Number
Cumulative (%)
Interval (ns)
0
10
20
30
40
0
25
50
75
100
0 20 40 60 80 100 120 140 160 180 200 220 240 260

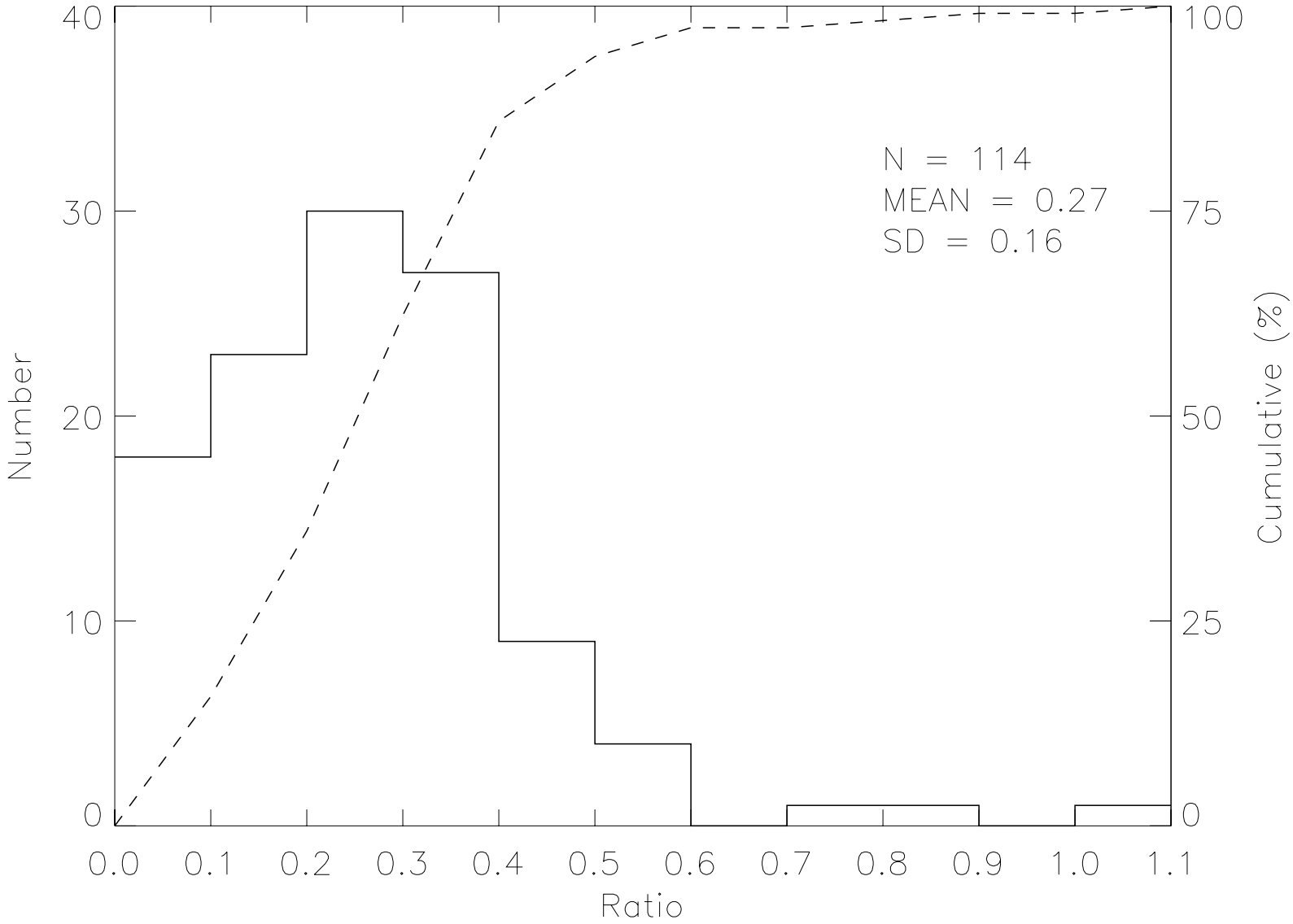
N = 114
MEAN = 0.27
SD = 0.16
Number
Cumulative (%)
Ratio
0
10
20
30
40
0
25
50
75
100
0.0
0.1
0.2
0.3
0.4
0.5
0.6
0.7
0.8
0.9
1.0
1.1

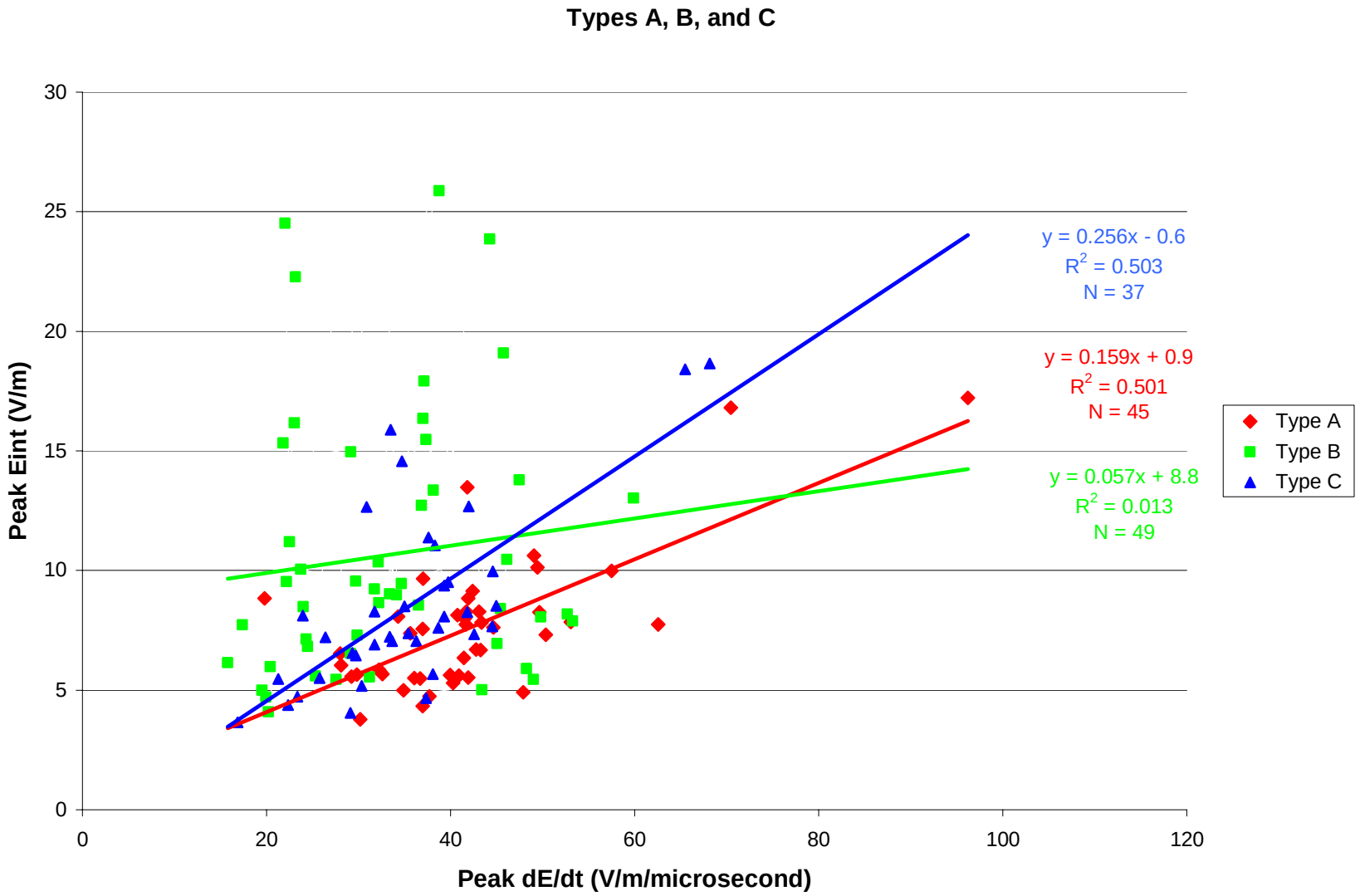
Types A, B, and C
Peak Eint (V/m)
Peak dE/dt (V/m/microsecond)
0
5
10
15
20
25
30
0
20
40
60
80
100
120
y = 0.256x - 0.6
R2 = 0.503
N = 37
y = 0.159x + 0.9
R2 = 0.501
N = 45
y = 0.057x + 8.8
R2 = 0.013
N = 49
Type A
Type B
Type C

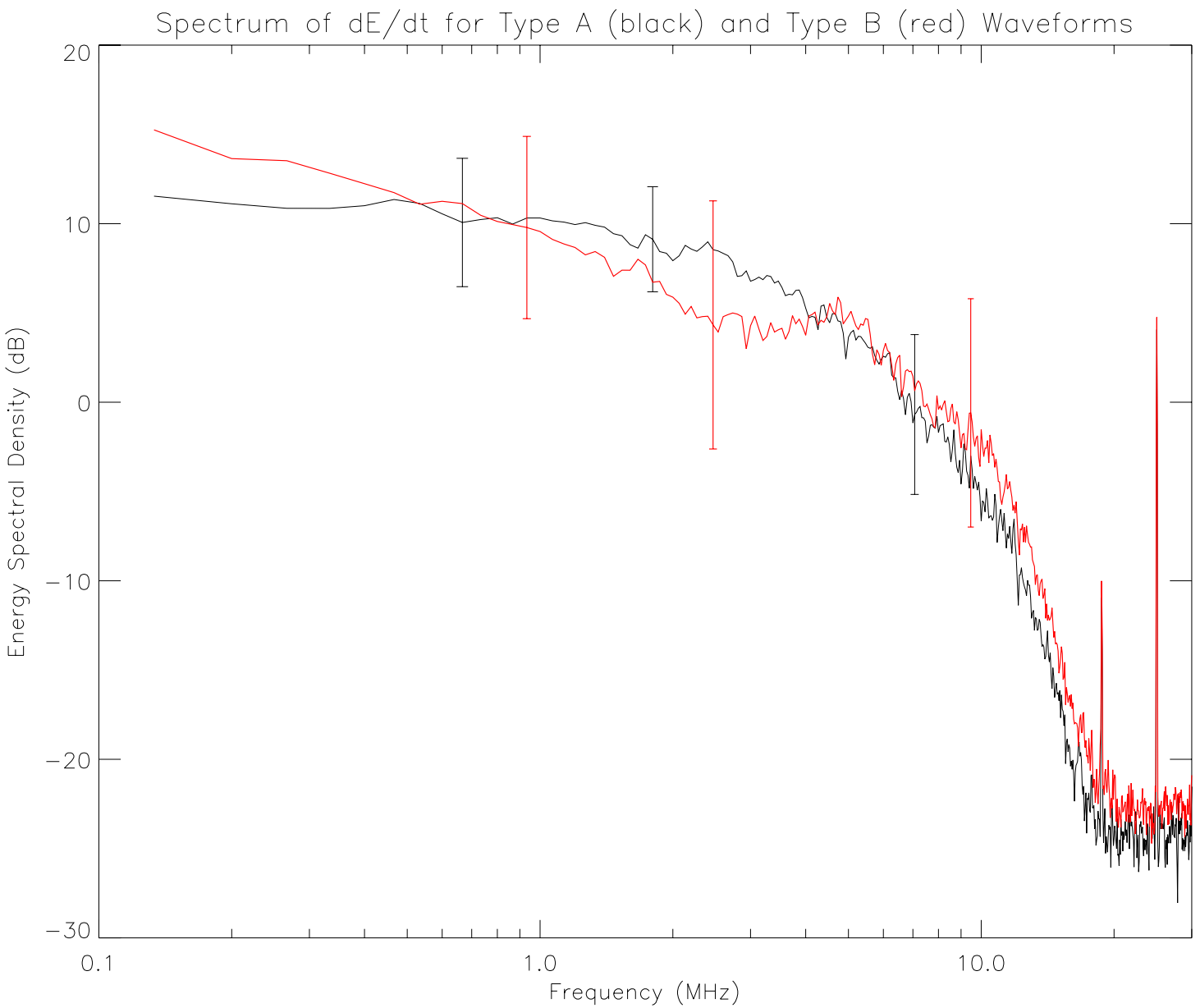
Spectrum of dE/dt for Type A (black) and Type B (red) Waveforms
20
10
0
−10
−20
−30
Energy Spectral Density (dB)
0.1
1.0
10.0
Frequency (MHz)

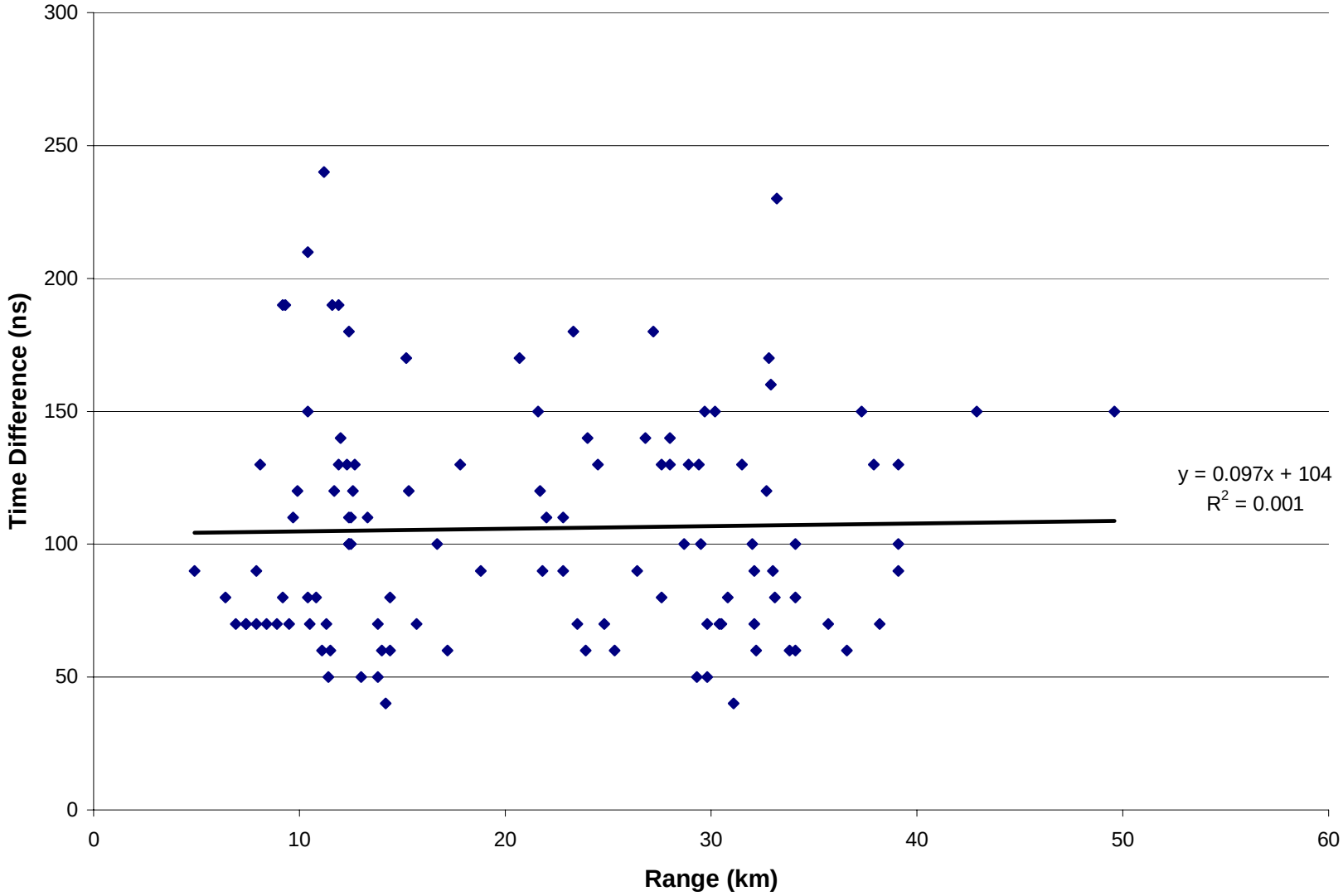
Time Difference (ns)
300
250
200
150
100
50
0
0
10
20
30
40
50
60
Range (km)
y = 0.097x + 104
R2 = 0.001

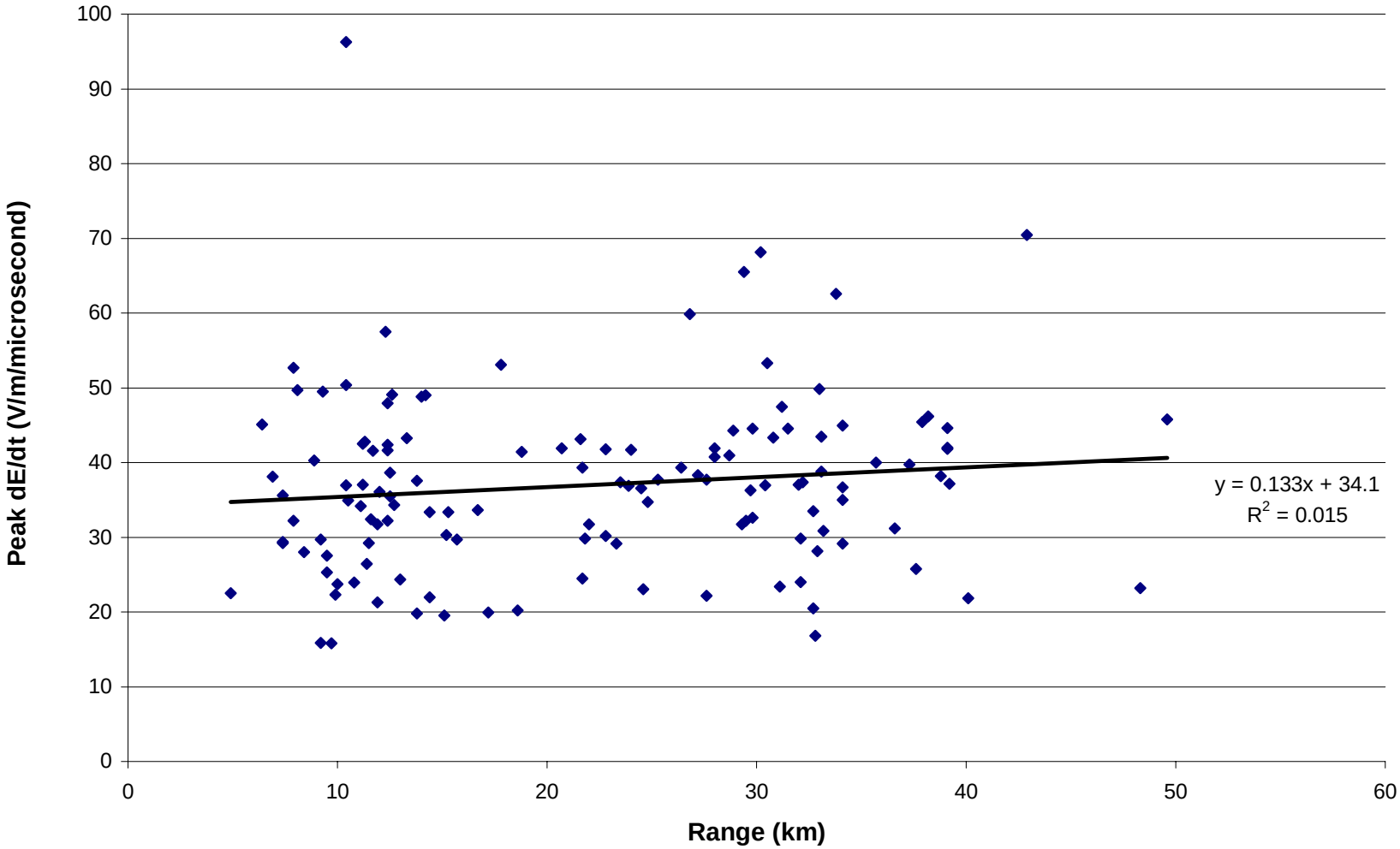
Peak dE/dt (V/m/microsecond)
100
90
80
70
60
50
40
30
20
10
0
0
10
20
30
40
50
60
Range (km)
y = 0.133x + 34.1
R2 = 0.015